

Invited review article

Triple oxygen isotopes in the water cycle

Phoebe G. Aron^{a,*}, Naomi E. Levin^a, Emily J. Beverly^b, Tyler E. Huth^a, Benjamin H. Passey^a,
Elise M. Pelletier^a, Christopher J. Poulsen^a, Ian Z. Winkelstern^c, Drake A. Yarian^a

^a Department of Earth and Environmental Sciences, University of Michigan, Ann Arbor, MI 48109, United States

^b Department of Earth and Atmospheric Sciences, University of Houston, Houston, TX, 77204, United States

^c Department of Geology, Grand Valley State University, Allendale, MI, 49401, United States

ARTICLE INFO

Editor: Michael E. Boettcher

Keywords:

Triple oxygen isotopes

Meteoric water

Mass-dependent fractionation

ABSTRACT

The past decade has seen a remarkable expansion of studies that use mass-dependent variations of triple oxygen isotopes (^{16}O , ^{17}O , ^{18}O) in isotope hydrology and isotope geochemistry. Recent technological and analytical advances demonstrate that small deviations of $\delta^{18}\text{O}$ and $\delta^{17}\text{O}$ from a mass-dependent reference relationship are systematic and are explained by well-known equilibrium and kinetic fractionations. Measurements of $\delta^{18}\text{O}$ and $\delta^{17}\text{O}$ complement traditional metrics like deuterium-excess, constrain isotope effects of kinetic fractionation that are impossible to discern with $\delta^{18}\text{O}$ alone, and help reconstruct past environmental conditions from geologic records. In this review, we synthesize published meteoric (derived from precipitation) water triple oxygen isotope data with a new, near-global surface water dataset of $\delta^{18}\text{O}$, $\delta^{17}\text{O}$, $\delta^2\text{H}$, deuterium-excess, and $\Delta^{17}\text{O}$, where $\Delta^{17}\text{O}$ is defined as $\delta^{17}\text{O} - \lambda_{\text{ref}} \delta^{18}\text{O}$, δ' notation is a logarithmic definition of the common δ value ($\delta' = \ln(\delta + 1)$), and λ_{ref} is equal to 0.528. The expanded dataset shows that meteoric water $\delta^{18}\text{O}$ and $\delta^{17}\text{O}$ fit multiple regression lines and indicates that one global meteoric water line does not adequately describe all triple oxygen isotope data. Instead, this isotope system may be sensitive to processes such as moisture transport, rainout, and evaporation that do not affect the water cycle equally across the globe. This review provides a practical guide to understand $\Delta^{17}\text{O}$ variation in waters, explains the utility of this isotope system in hydrologic and paleoclimate studies, and outlines directions of future work that will expand the use of $\Delta^{17}\text{O}$.

1. Introduction

Ratios of ^{18}O to ^{16}O are among the most common isotopic measurements in Earth science and play a critical role tracing biogeochemical cycles and reconstructing past climate conditions (Dansgaard, 1964; Joussauze et al., 1984; Zachos, 2001). Studies of ^{17}O , the rarest stable oxygen isotope (Table 1), have lagged because $^{17}\text{O}/^{16}\text{O}$ ratios were long considered invariant, too difficult to measure, or redundant to $^{18}\text{O}/^{16}\text{O}$ ratios (Gat, 1996). However, recent technological and analytical advances show that small, mass-dependent deviations between $^{17}\text{O}/^{16}\text{O}$ and $^{18}\text{O}/^{16}\text{O}$ contain new information about water cycling and past environmental conditions (Barkan and Luz, 2005). This review captures the emerging field of triple oxygen isotope (^{16}O , ^{17}O , ^{18}O) hydrology at an important moment: many laboratories are now able to make ^{17}O measurements and large datasets are rapidly emerging, but triple oxygen isotope variability is not yet fully understood and there are important inconsistencies between studies. Therefore, this review

synthesizes new and published meteoric (derived from precipitation) water isotope data and explains the processes that drive triple oxygen isotope variation in the water cycle. This review is intended as an introduction to triple oxygen isotope hydrology and as a primer to how this emerging field may contribute to hydrologic and paleoclimate research.

Oxygen isotopes fractionate due to non-mass-dependent and mass-dependent effects (Bao et al., 2016; Thiemens et al., 2012). Non-mass-dependent fractionation arises from chemical effects, including nuclear spin, transition state chemistry, molecular symmetry, and photochemical reactions (Criss and Farquhar, 2008; Thiemens and Heidenreich, 1983). These effects can result in large variations between $^{17}\text{O}/^{16}\text{O}$ and $^{18}\text{O}/^{16}\text{O}$ and have a range of applications in atmospheric chemistry, planetary science, and biological productivity that are already well reviewed (Bao et al., 2009; Bhattacharya et al., 2000; Blunier et al., 2012; Blunier et al., 2002; Luz et al., 2009; Thiemens, 2006; Thiemens et al., 1995). In contrast, mass-dependent effects arise

* Corresponding author.

E-mail address: paron@umich.edu (P.G. Aron).

Table 1
The three stable oxygen isotopes.

Isotope	Symbol	Protons	Neutrons	Mass (u)	Natural terrestrial abundance (%)
Oxygen-16	^{16}O	8	8	15.995	99.757
Oxygen-17	^{17}O	8	9	16.999	0.038
Oxygen-18	^{18}O	8	10	17.999	0.205

from differences in bond energy, reaction rate, and diffusivity (Matsuhisa et al., 1978; Young et al., 2002) that result in very small variations between $^{17}\text{O}/^{16}\text{O}$ and $^{18}\text{O}/^{16}\text{O}$. These mass-dependent variations are sensitive to fractionation during equilibrium isotope exchange and the diffusion of water vapor through air, and have recently gained attention as a new way to study modern hydrology and reconstruct past environmental conditions (e.g., Bao et al., 2016; Barkan and Luz, 2005; Luz and Barkan, 2010; Paek and Herwartz, 2014; Rumble et al., 2007).

Decoupling fractionation effects from equilibrium and kinetic processes is critical to interpreting isotope data and identifying processes such as Rayleigh distillation and evaporation. In modern waters, the degree of kinetic fractionation is often quantified using deuterium-excess ($d\text{-excess} = \delta^2\text{H} - 8 \cdot \delta^{18}\text{O}$, Dansgaard, 1964; see Section 2.1 for the definition of δ notation). However, $d\text{-excess}$ varies with both temperature and relative humidity, so interpretations of $d\text{-excess}$ data are not always straightforward (Gat, 1996). Mass-dependent variations between $^{17}\text{O}/^{16}\text{O}$ and $^{18}\text{O}/^{16}\text{O}$ can also quantify kinetic fractionation, but are relatively insensitive to temperature (Barkan and Luz, 2005). Therefore, triple oxygen isotopes and $d\text{-excess}$ provide complementary information to track evapotranspiration, moisture transport, and precipitation processes (e.g., Galewsky et al., 2016), identify temperature and relative humidity conditions at moisture sources (Landais et al., 2008, 2012a, 2012b; Uemura et al., 2010; Winkler et al., 2012), and link seasonal or glacial-interglacial isotope cycles to climate conditions (Risi et al., 2010; Schoenemann and Steig, 2016).

Translating these principles to the past and differentiating equilibrium and kinetic fractionation effects in paleoclimate records is challenging because most geologic archives (e.g., carbonates, sulfates, phosphates, etc.) do not have both oxygen- and hydrogen-containing minerals. Much like $d\text{-excess}$ (Fig. 1), triple oxygen isotopes add a degree of freedom ($^{17}\text{O}/^{16}\text{O}$) to paleoclimate records and can clarify some processes and fractionations that cannot be resolved with traditional oxygen isotope ratios ($^{18}\text{O}/^{16}\text{O}$) alone (e.g., Rech et al., 2019). For example, triple oxygen isotope ratios preserved in minerals add new information about aridity and paleo-humidity (Alexandre et al., 2019; Gázquez et al., 2018; Passey and Ji, 2019; Surma et al., 2018), enable reconstructions of the isotopic composition of ancient waters (e.g., Gehler et al., 2011; Herwartz et al., 2015; Liljestrand et al., 2020; Passey and Ji, 2019), and constrain effects of diagenesis and formation conditions of sedimentary records (Levin et al., 2014).

Clearly the potential applications of triple oxygen isotopes in hydrology and paleoclimate are immense. However, this field is still relatively young, global variations are not yet well characterized, and explanations of triple oxygen isotope variability are scattered among the literature (Table 2) or are not well understood. The seminal description of modern meteoric water triple oxygen isotopes (Luz and Barkan, 2010) laid the foundation for a decade of research (Fig. 2 and Table 2), but there is now far more variability than initially realized (Fig. 3a and b) and triple oxygen isotope ratios do not neatly fit a global meteoric water line (Sharp et al., 2018). Therefore, building upon more than a decade of work, this review re-examines meteoric water $\delta^{18}\text{O}$, $\delta^{17}\text{O}$, $\delta^2\text{H}$, $\Delta^{17}\text{O}$, and $d\text{-excess}$ data. We synthesize published and new meteoric water data to evaluate the $\delta^{18}\text{O}$ - $\delta^{17}\text{O}$ relationship (Section 5), explain the hydrologic processes and mass-dependent fractionations that drive variation in $\Delta^{17}\text{O}$ and $d\text{-excess}$ (Section 6), review analytical methods and considerations for $\Delta^{17}\text{O}$ measurements (Section 7), and present directions of future triple oxygen isotope work (Section 9).

2. Isotope terminology and fractionation

A summary of common symbols, explanations, and values in hydrologic triple oxygen isotope studies is provided in Table 3.

2.1. Isotope notation

Isotope partitioning between two substances (A and B) is expressed as an isotopic fractionation factor, α :

$$\alpha_{A-B} = R_A/R_B \quad (1)$$

where R is the ratio of the rare to common isotope (e.g., $^2\text{H}/^1\text{H}$, $^{18}\text{O}/^{16}\text{O}$, or $^{17}\text{O}/^{16}\text{O}$). During a single mass-dependent fractionating process, α values of coexisting phases (e.g., liquid and vapor), materials (e.g., water and mineral), or components related by simple processes (e.g., diffused gas and residual gas) are related by a power law relationship derived from mass law theory (Matsuhisa et al., 1978; Young et al., 2002):

$${}^*\alpha_{A-B} = ({}^*\alpha_{A-B})^\theta \quad (2)$$

where θ , the fractionation exponent, is a constant that defines the relationship between α values and * denotes a heavy mass number (e.g., 17 or 18 for oxygen, 2 for hydrogen).

Triple oxygen isotope fractionation exponents are well characterized for equilibrium (θ_{eq}) and kinetic (θ_{diff}) processes. Liquid-vapor θ_{eq} is predicted by mass law theory (Young et al., 2002, $\theta_{\text{eq}} = 0.529$) and has been verified empirically (Barkan and Luz, 2005, $\theta_{\text{eq}} = 0.529 \pm 0.001$); the kinetic fractionation exponent for diffusion of water vapor through air (θ_{diff}) is derived from the kinetic theory of gases and the ideal gas law

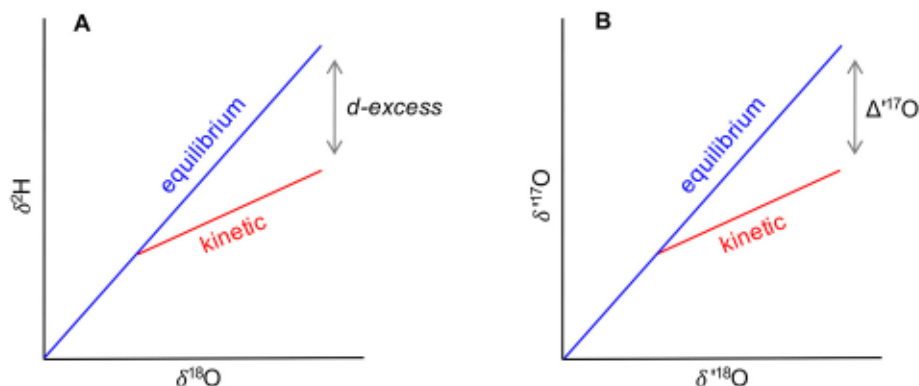


Fig. 1. Schematic showing the similarities between (A) $d\text{-excess}$ and (B) $\Delta^{17}\text{O}$. Note that $\Delta^{17}\text{O}$ is defined from $\delta^{18}\text{O}$ and $\delta^{17}\text{O}$. See Eq. (4) for the definition of δ' notation

Table 2
Summary of published hydrologic triple oxygen water isotope studies.

Water type	Timeframe	Location	Analysis method	Reference
Plant Water				
Leaf	April 2015	Europe and Israel	IRMS	Landais et al., 2006
Stem and leaf	Summer 2012	Central Kenya	IRMS	Li et al., 2017
Meteoric Water				
Various	Various, 2002-2010	global	IRMS	Luz and Barkan, 2010
Precipitation	Seasonal, short convective cell	Niger	IRMS	Landais et al., 2010
Surface water	Spring 2011	Iran	IRMS	Surma et al., 2015
Tap water	2008-2011	Continental United States	IRMS	Li et al., 2015
Precipitation, cave drip	March 2012-July 2014	Switzerland	Picarro	Affolter et al., 2015
Precipitation, surface water, cave drip	2012-2013	Spain	Picarro	Gazquez et al., 2017
Surface water	March 2014	Atacama Desert, Chile	IRMS	Surma et al., 2018
Precipitation	Event scale, 2014-2018	Central United States	LGR	Tian et al., 2018, Tian et al., 2019
Precipitation	Event scale, 2012-2016	Namibia	LGR	Kaseke et al., 2018
Tap water	Monthly, December 2014 to November 2015	China	LGR	Tian et al., 2019
Precipitation	Weekly, January 2011 to December 2012	Japan	Picarro	Uechi and Uemura, 2019
Surface water	June 2014	Western United States	IRMS	Passey and Ji, 2019
Surface water	2017-2018	Northern Israel	IRMS	Bergel et al., 2020
Surface water and ocean	2015-2016	Pacific Northwest, United States	Picarro	Bershaw et al., 2020
Surface water	Various, 2016-2019	global	IRMS	this study
Polar Precipitation				
Snow and ice	Last 150,000 years	Vostok, Antarctica	IRMS	Landais et al., 2008
Snow	2000	Vostok, Antarctica	IRMS	Landais et al., 2012a
Snow and water vapor	2003-2005	Greenland	IRMS	Landais et al., 2012b
Ice	Glacial-interglacial cycles	East Antarctica	IRMS	Winkler et al., 2012
Ice	LGM to Holocene	WAIS Divide, Antarctica	IRMS	Schoenemann et al., 2014
Snow	December 2009-January 2010	Coast to Dome A transect, East Antarctica	IRMS	Pang et al., 2015
Snow	1999-2011	East Antarctica	IRMS	Touzeau et al., 2016
Snow	January 2010	East Antarctica	IRMS	Pang et al., 2019
Modeling				
Vapor	Glacial-interglacial cycles	Vostok, Antarctica	Single column model	Risi et al., 2010
Precipitation	Modern and LGM	global	LMDZ (atmospheric transport GCM)	Risi et al., 2013
Precipitation	Modern seasonal cycle	Antarctica	Intermediate complexity model	Schoenemann and Steig, 2016

Analysis method abbreviations: isotope ratio mass spectrometer (IRMS), Los Gatos Research (LGR), Laboratory of Dynamic Meteorology (LMDZ), general circulation model (GCM).

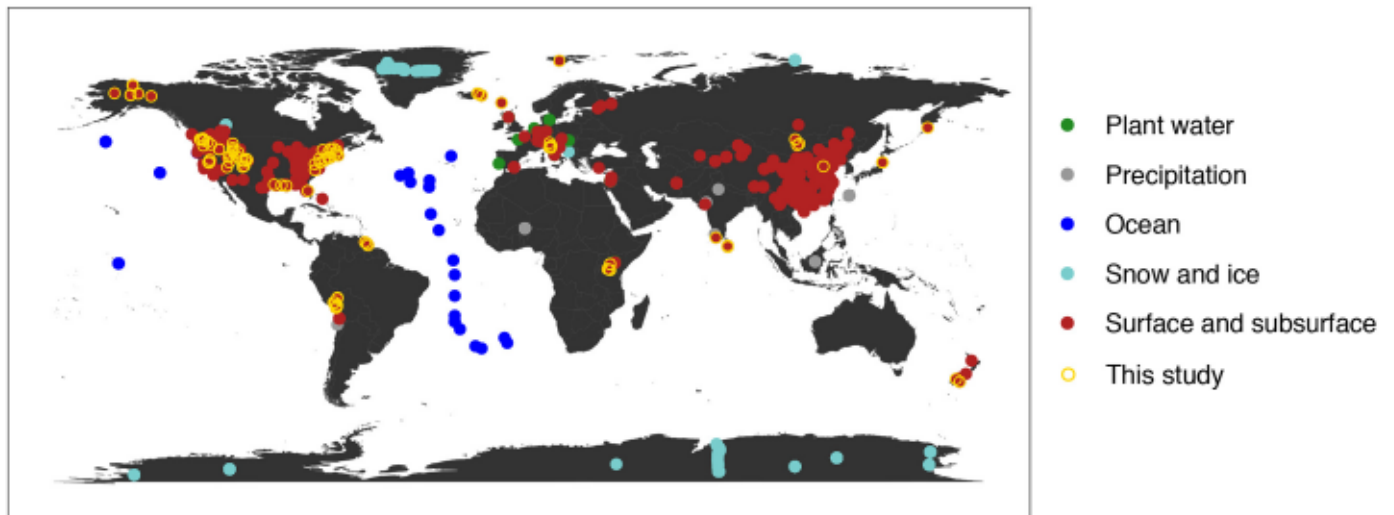


Fig. 2. Geographical distribution of published meteoric water triple oxygen isotope data, colored by sample type. Plant water includes water extracted from stems and leaves. Surface and subsurface includes surface water, soil water, groundwater, cave water, and tap water. New surface water samples reported in this review are outlined in gold; published studies are listed in Table 2.

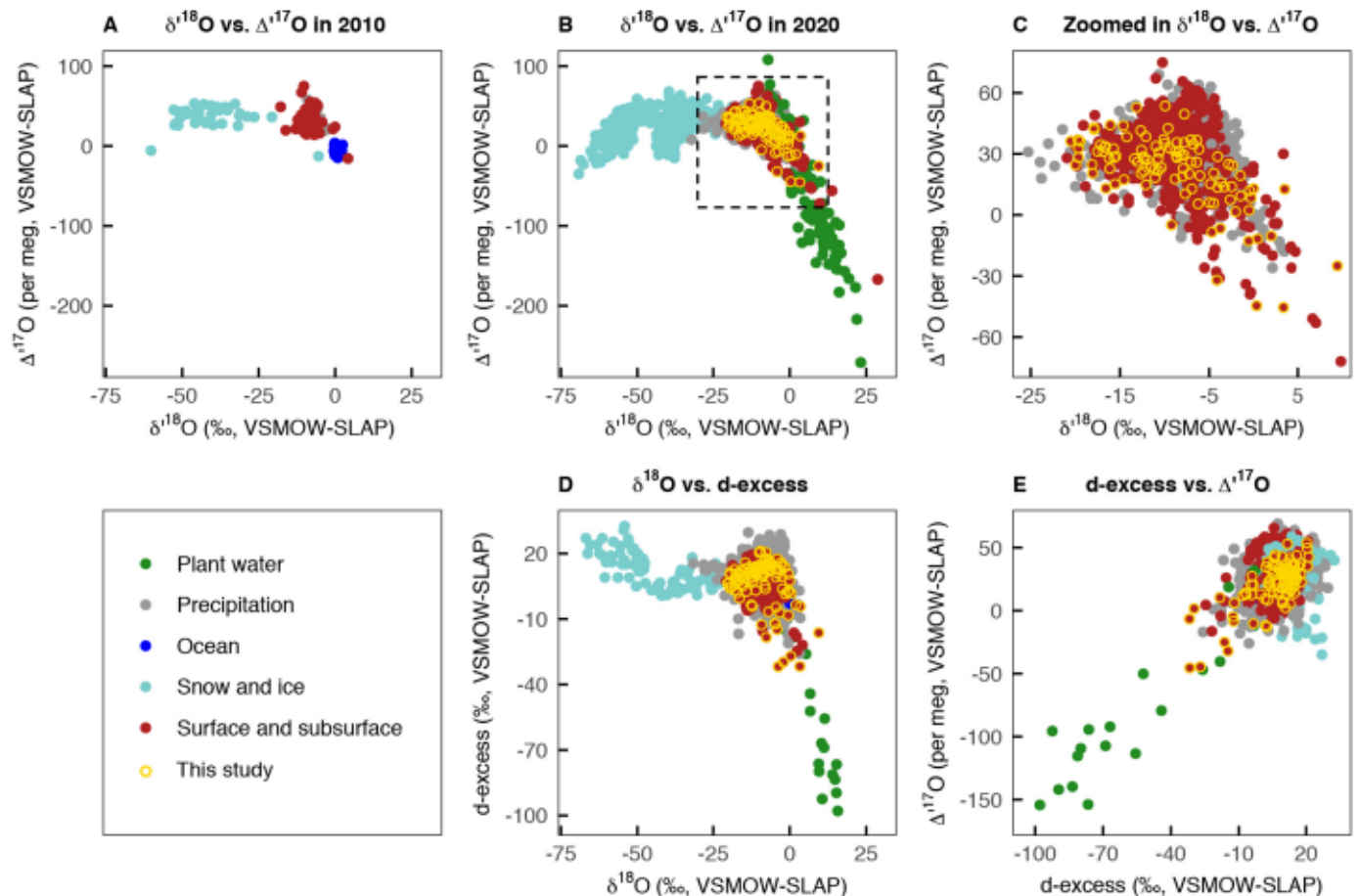


Fig. 3. Scatterplots of meteoric water isotope data. Color indicates sample type. New surface water data reported in this study are outlined in gold. The top row shows plots of $\delta^{18}\text{O}$ versus $\Delta^{17}\text{O}$ from (A) Luz and Barkan (2010), (B) all published data as of 2020 (Table 2), and (C) published precipitation, surface, and subsurface waters within a normal meteoric range (-25 to 10‰) as of 2020. The dashed box in (B) outlines the limits of the data in (C). The bottom row shows plots of (D) $\delta^{18}\text{O}$ versus d-excess and (E) d-excess versus $\Delta^{17}\text{O}$ from all the available published meteoric water triple oxygen isotope data (Table 2). There are more points in (B) than (D) or (E) because not all studies include $\delta^2\text{H}$ data.

Table 3
Common symbols, explanations, and values for triple oxygen isotopes.

Symbol	Value	Explanation	Reference
ϵ_{eq}	0.529	liquid-vapor equilibrium fractionation exponent	Barkan and Luz, 2005
ϵ_{diff}	0.518	water vapor diffusion fractionation exponent	Barkan and Luz, 2007
α_{eq}^{18}	Variable (temperature dependent)	$^{18}\text{O}/^{16}\text{O}_{\text{l-v}}$ equilibrium fractionation factor	Majoube, 1971
α_{eq}^{17}	α_{eq}^{18}	$^{17}\text{O}/^{16}\text{O}_{\text{l-v}}$ equilibrium fractionation factor	Eq. (2)
$\alpha_{\text{diff}}^{18}$	1 (pure turbulent transport) to 1.0285 (transport via pure molecular diffusion)	$^{18}\text{O}/^{16}\text{O}_{\text{l-v}}$ diffusive transport fractionation factor	Merlivat, 1978
$\alpha_{\text{diff}}^{17}$	$\alpha_{\text{diff}}^{18}$	$^{17}\text{O}/^{16}\text{O}_{\text{l-v}}$ diffusive transport fractionation factor	Eq. (2)
λ_{ref}	0.528	slope of the ^{18}O ^{17}O reference line commonly used in hydrologic studies	Luz and Barkan, 2010
	$\frac{R_{\text{sample}}}{R_{\text{standard}}}$	delta	McKinney et al., 1950
	$\ln\left(\frac{R_{\text{sample}}}{R_{\text{standard}}}\right)$	delta prime	Hulston and Thode, 1965; Miller, 2002
$\Delta^{17}\text{O}$	$\Delta^{17}\text{O}$	cap ^{17}O	Barkan and Luz, 2007

(Marrero and Mason, 1972, ϵ_{diff} 0.5184) and has also been confirmed experimentally (Barkan and Luz, 2007, ϵ_{diff} 0.5185 0.0003). The small, but statistically significant, difference between ϵ_{eq} and ϵ_{diff} values means that triple oxygen isotopes can differentiate equilibrium and kinetic fractionation in materials that contain oxygen atoms.

In nature, isotopic compositions rarely reflect fractionation from a single process, but instead integrate multiple fractionating processes and several values. Following convention from triple oxygen isotope literature, we use notation to differentiate relationships that integrate multiple fractionating processes () from those that result from a single fractionating process (). The most familiar value in isotope hydrology is the slope (~ 8) of the oxygen-hydrogen global meteoric water line, ^2H $8^* ^{18}\text{O}$ 10 (Craig, 1961), where notation is expressed in per mil and defined as

$$\epsilon = \left(\frac{R_{\text{sample}}}{R_{\text{standard}}} - 1 \right) \times 1000 \quad (3)$$

Linear meteoric water isotope relationships are ubiquitous in isotope hydrology because they provide a useful reference frame from which to assess isotopic variability and quantify non-equilibrium fractionation (Gat, 1996). However, these relationships are not always truly linear because mass-dependent fractionation follows a power law function (Eq. (2)). This non-linearity is rarely observed in natural waters (e.g., Craig, 1961; Dansgaard, 1964; Rozanski et al., 1993) because the range of isotope values on Earth is relatively small and the scatter of data points around an apparent linear relationship is too great to resolve the slight curvature (Fig. 4a and c). However, curvature appears over a sufficiently large isotopic range (Fig. 4b and d). This curvature is concave when the slope between isotopic compositions is greater than 1 (Fig. 4b) and convex when the slope between isotopic compositions is less than 1 (Fig. 4d). Logarithmic (delta prime) notation linearizes the exponential relationship between isotopic compositions (Fig. 4b and d; Hulston and Thode, 1965; Miller, 2002):

$$\epsilon' = \ln\left(\frac{R_{\text{sample}}}{R_{\text{standard}}}\right) \quad (4)$$

This notation is used in all triple oxygen isotope studies and some studies of d-excess (e.g., Dütsch et al., 2017).

2.2. Definition of $\Delta^{17}\text{O}$

Compilations of ^{18}O and ^{17}O almost always appear linear (Fig. 4c), so the most practical way to view and interpret triple oxygen isotope data is as a deviation from a reference line (Barkan and Luz, 2007):

$$\Delta^{17}\text{O} = \left(\frac{R_{\text{sample}}}{R_{\text{reference}}} - \lambda_{\text{ref}} \right) \times 1000 \quad (5)$$

In this definition, λ_{ref} is the slope of a mass-dependent reference line and notation ensures that isotopic deviations are calculated from a ^{18}O ^{17}O relationship that is exactly linear. This notation is critical because a non-linear calculation artifact biases $\Delta^{17}\text{O}$ when ^{18}O and ^{17}O values are used instead of ^{18}O and ^{17}O values (Fig. 5). d-excess

also varies non-linearly when it is defined with notation, but a logarithmic definition of d-excess is typically considered only at high latitudes or when ^{18}O variation is large (Dütsch et al., 2017; Schoenemann et al., 2014; Uemura et al., 2012). The notation is imperative for triple oxygen isotopes because the non-linear $\Delta^{17}\text{O}$ calculation artifact is the same order of magnitude as analytical $\Delta^{17}\text{O}$ precision and natural $\Delta^{17}\text{O}$ variability in the water cycle (Fig. 5). The slope of the ^{18}O ^{17}O reference line is discussed in Section 5, but hydrologic studies, including this review, typically use a value of 0.528 for λ_{ref} . Values of $\Delta^{17}\text{O}$ are generally very small and are expressed in units of per meg (1,000 per meg ‰).

The triple oxygen isotope literature uses multiple terms to express ^{18}O and ^{17}O deviations from the reference relationship in waters. For example, $\Delta^{17}\text{O}$, $\Delta^{17}\text{O}$, ^{17}O -excess, and $^{17}\text{O}_{\text{excess}}$ are all found in triple oxygen isotope literature (Sharp et al., 2018; Passey and Ji, 2019; Luz and Barkan, 2010; Landais et al., 2010, respectively). These terms are equivalent and are each defined as in Eq. (5) in this review, but the different notation can cause confusion among studies. The ^{17}O -excess and $^{17}\text{O}_{\text{excess}}$ terms are advantageous because they highlight the relative excess of ^{17}O in meteoric waters as compared to ocean water and emphasize similarities between the triple oxygen isotope system and d-excess (Fig. 1). The capital delta notation is advantageous because Δ notation is defined as the isotopic deviation from a reference relationship and is used in multiple isotope systems (e.g., $\Delta^{34}\text{S}$ and $\Delta^{25}\text{Mg}$; Criss and Farquhar, 2008; Young and Galy, 2004).

We prefer and recommend the $\Delta^{17}\text{O}$ term (Eq. (5) and Sharp et al., 2018) because this notation explicitly indicates that the $\Delta^{17}\text{O}$ parameter is calculated using values (not values) and defines this parameter as the deviation from a reference relationship.

3. Motivation from a decade of $\Delta^{17}\text{O}$ observations

Meteoric water isotope patterns are best observed from amount-weighted precipitation (Dansgaard, 1964; Rozanski et al., 1993) or flowing surface waters (Kendall and Coplen, 2001) because these waters integrate fractionating processes in the hydrosphere, atmosphere, and biosphere. Efforts to understand patterns in ^{18}O and ^2H have culminated in the global meteoric water line (Craig, 1961), ^{18}O and ^2H isoscapes (e.g., Bowen, 2010), and well-tuned isotope-enabled general circulation models (Brady et al., 2019; Joussaume et al., 1984) that reflect ^{18}O and ^2H variations across almost every region on Earth. These products are a point of reference for nearly every hydrologic and paleoclimate study of ^{18}O and ^2H (e.g., Jasechko, 2019; Noone et al., 2013; Poulsen et al., 2010; Rowley and Garzzone, 2007).

Comprehensive global and continent scale water isotope studies such as those by Craig (1961), Dansgaard (1964), Rozanski et al. (1993), and Kendall and Coplen (2001) do not yet exist for triple oxygen isotopes. Global variability of meteoric water $\Delta^{17}\text{O}$ and ^{18}O was first described in 2010 from a dataset comprised of two international standards, SLAP (Standard Light Antarctic Precipitation) and GISP (Greenland Ice Sheet Precipitation) (Barkan and Luz, 2005); 29 Antarctic snow samples

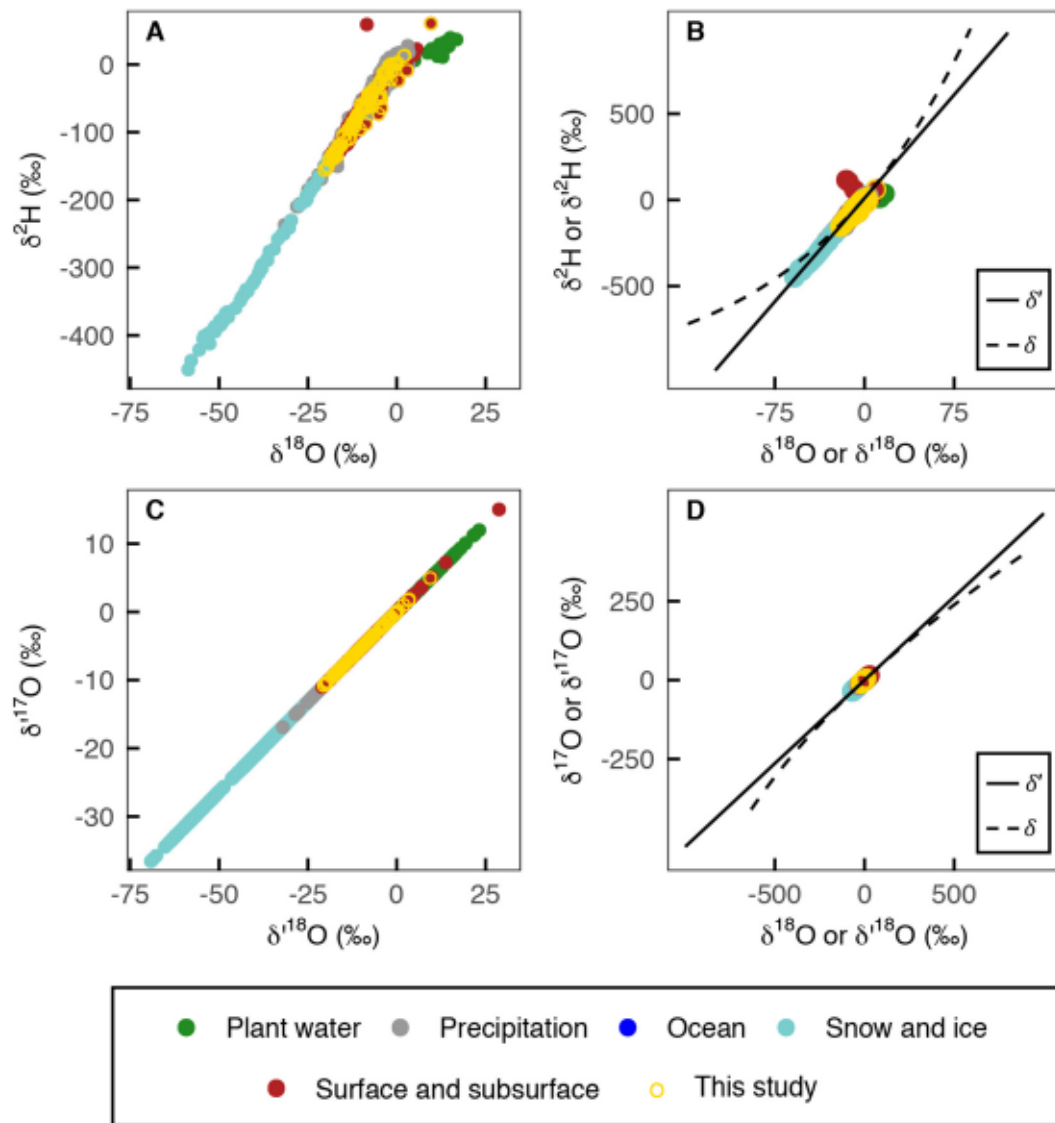


Fig. 4. Scatterplots of meteoric water isotope values. Published data (Table 2) are colored by sample type; new data reported in this review are outlined in gold. Over the natural range of (A) $\delta^{18}\text{O}$ versus $\delta^2\text{H}$ and (C) $\delta^{18}\text{O}$ versus $\delta^{17}\text{O}$, meteoric water isotope relationships are nearly linear. The same data are shown in (B) and (D), respectively, but are overlaid with calculated $\delta^{18}\text{O}$, $\delta^{17}\text{O}$, or $\delta^2\text{H}$ (dashed black line) and calculated $\delta^{18}\text{O}$, $\delta^{17}\text{O}$, or $\delta^2\text{H}$ (solid black line) over larger isotopic ranges. There are fewer points in (A) and (B) than (C) and (D) because some triple oxygen isotope studies do not include $\delta^2\text{H}$ data. The curvature between δ - δ relationships is concave when the slope between isotope values is greater than 1 (B, $\delta^{18}\text{O}$ - $\delta^2\text{H}$) and convex when the slope between isotope values is less than 1 (D, $\delta^{18}\text{O}$ - $\delta^{17}\text{O}$).

(Landais et al., 2008); and 52 meteoric waters from locations mostly scattered throughout Europe and Asia (Luz and Barkan, 2010). From this compilation, Luz and Barkan (2010) defined a global meteoric water line, established λ_{ref} as the slope of this line, and set the expectation that $\Delta^{17}\text{O}$ values of meteoric water should be relatively invariant over a $\sim 70\%$ range in $\delta^{18}\text{O}$ (Fig. 3a). However, observations since this seminal work show that meteoric water $\Delta^{17}\text{O}$ is far more variable than initially recognized (compare Fig. 3a and b). Moreover, the meteoric water $\delta^{18}\text{O}$ and $\delta^{17}\text{O}$ data published since 2010 can fit multiple regression lines, suggesting that the global meteoric water line defined in 2010 may not actually represent global meteoric waters (Miller, 2018; Sharp et al., 2018).

We use this review paper to provide both a synopsis of what we know about $\delta^{18}\text{O}$, $\delta^{17}\text{O}$, and $\Delta^{17}\text{O}$ in meteoric water and as a guide for how practitioners might use triple oxygen isotope data in hydrologic and paleoclimate studies. As part of this review, we report a new, near-global surface water dataset that spans 6 continents and 17 Köppen climate classes and expands the published meteoric water triple oxygen isotope dataset. In the following sections we 1) introduce our new surface water

data, 2) evaluate the global $\delta^{18}\text{O}$ - $\delta^{17}\text{O}$ relationship and present updated triple oxygen isotope meteoric water relationships that better fit the available data, and 3) explain the hydrologic processes that drive $\Delta^{17}\text{O}$ variation in the water cycle. Following the framework established by Craig (1961), Dansgaard (1964), Rozanski et al. (1993), and Kendall and Coplen (2001), we prefer a narrow definition of meteoric water that includes only precipitation and surface water for the second objective. For the third objective, we include a much wider definition of meteoric water (plant water, precipitation, surface and subsurface, snow and ice, and ocean water) to explain triple oxygen isotope variation in as many parts of the hydrosphere as possible.

4. New surface water data

The new surface water dataset reported in this review includes $\delta^{18}\text{O}$, $\delta^{17}\text{O}$, $\delta^2\text{H}$, d-excess, and $\Delta^{17}\text{O}$ data from 104 rivers and lakes (Fig. 2). The samples are part of a global crowdsourced dataset, and the isotope data are reported in Supplements 1–3 and Figs. 3, 4, and 6. These data are briefly summarized here because they are included in the evaluation

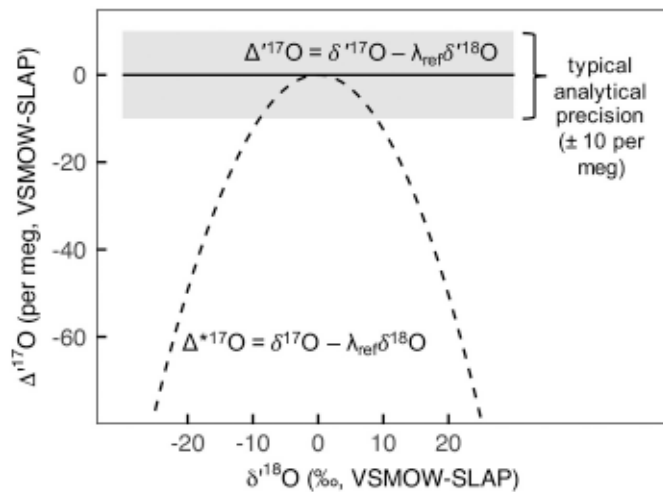


Fig. 5. Comparison of $\Delta^{17}\text{O}$ (solid black line) versus $\Delta^{*17}\text{O}$ (dashed black line) across a common range of meteoric water $\delta^{18}\text{O}$ values. The gray bar shows typical $\Delta^{17}\text{O}$ analytical precision (± 10 per meg). Note that $\Delta^{17}\text{O}$ is calculated with δ' values while $\Delta^{*17}\text{O}$ is calculated with δ values. Without δ' notation, $\Delta^{*17}\text{O}$ varies non-linearly as a function of $\delta^{18}\text{O}$, and introduces a bias in $\Delta^{*17}\text{O}$ that is greater than analytical precision and a similar magnitude to environmentally driven variability. δ' notation linearizes the definition of $\Delta^{17}\text{O}$ and removes the non-linear calculation artifact.

of the triple oxygen isotope meteoric water line (Section 5) and explanations of $\Delta^{17}\text{O}$ variability (Section 6). A complete description of our sample collection and analytical methods are in Section 8.

Briefly, the $\delta^{18}\text{O}$ and $\delta^2\text{H}$ values were measured with a Picarro L2130-i cavity ringdown spectrometer and $\delta^{18}\text{O}$ and $\delta^{17}\text{O}$ values were analyzed with a Nu Perspective isotope ratio mass spectrometer. All isotopic analyses were done at the University of Michigan. The analytical precision of the Picarro $\delta^{18}\text{O}$ and $\delta^2\text{H}$ measurements was determined from replicate injections of deionized water and was better than 0.1‰ and 0.3‰, respectively. The root mean square error (RMSE) of replicate Nu measurements of USGS reference waters was better than

0.3‰ for $\delta^{17}\text{O}$, 0.9‰ for $\delta^{18}\text{O}$, and 10 per meg for $\Delta^{17}\text{O}$. The analytical error on our measurements is nearly identical to all other published meteoric water isotope data.

4.1. Isotopic compositions of the new surface water dataset

Surface water $\delta^{18}\text{O}$ ranges from -20.3 to 9.6‰ , d-excess ranges from -31.8 to 21.1‰ , and $\Delta^{17}\text{O}$ ranges from -45 to 54 per meg, where $\Delta^{17}\text{O}$ is defined with λ_{ref} equal to 0.528 . Most isotopic compositions cluster between -14 to -5‰ , 3 to 13‰ , and 14 to 33 per meg ($\delta^{18}\text{O}$, d-excess, and $\Delta^{17}\text{O}$, respectively), but have high standard deviations (6.1‰ , 11.1‰ , and 18 per meg, respectively) and are poorly described by average values. Values of $\Delta^{17}\text{O}$ are moderately to strongly positively correlated with d-excess (Pearson's $r = 0.73$) and moderately to strongly negatively correlated with $\delta^{18}\text{O}$ ($r = -0.64$). Both $\Delta^{17}\text{O}$ and d-excess are very weakly correlated or uncorrelated with latitude, longitude, elevation, mean annual temperature, mean annual precipitation, and mean annual relative humidity (all $r < \pm 0.3$). Rivers tend to have lower $\delta^{18}\text{O}$, higher d-excess, and higher $\Delta^{17}\text{O}$ values than lakes, although some rivers and lakes in arid regions are isotopically similar (Supplement 1). The slope ($\lambda = 0.5262 \pm 0.0002$) through $\delta^{18}\text{O}$ and $\delta^{17}\text{O}$ values was determined from a Model II linear regression. The uncertainty on this slope, as well as all other slopes and intercepts throughout this review, is the standard error from a Model II linear regression. Climate data (mean annual precipitation, temperature, and relative humidity) from the sampling locations were extracted from the CRU 2.0 dataset (New et al., 2002) and are included in Supplement 1.

5. Triple oxygen isotope meteoric water lines and the reference slope

5.1. Triple oxygen isotope meteoric water lines

Meteoric water lines define the most fundamental relationships in isotope hydrology and provide a point of reference from which to interpret isotope data (e.g., Brooks et al., 2010; Craig, 1961; Jasechko, 2019). Here, we use the well-established $\delta^{18}\text{O}$ - $\delta^2\text{H}$ global meteoric water line (Craig, 1961) as a model to re-evaluate and update the triple

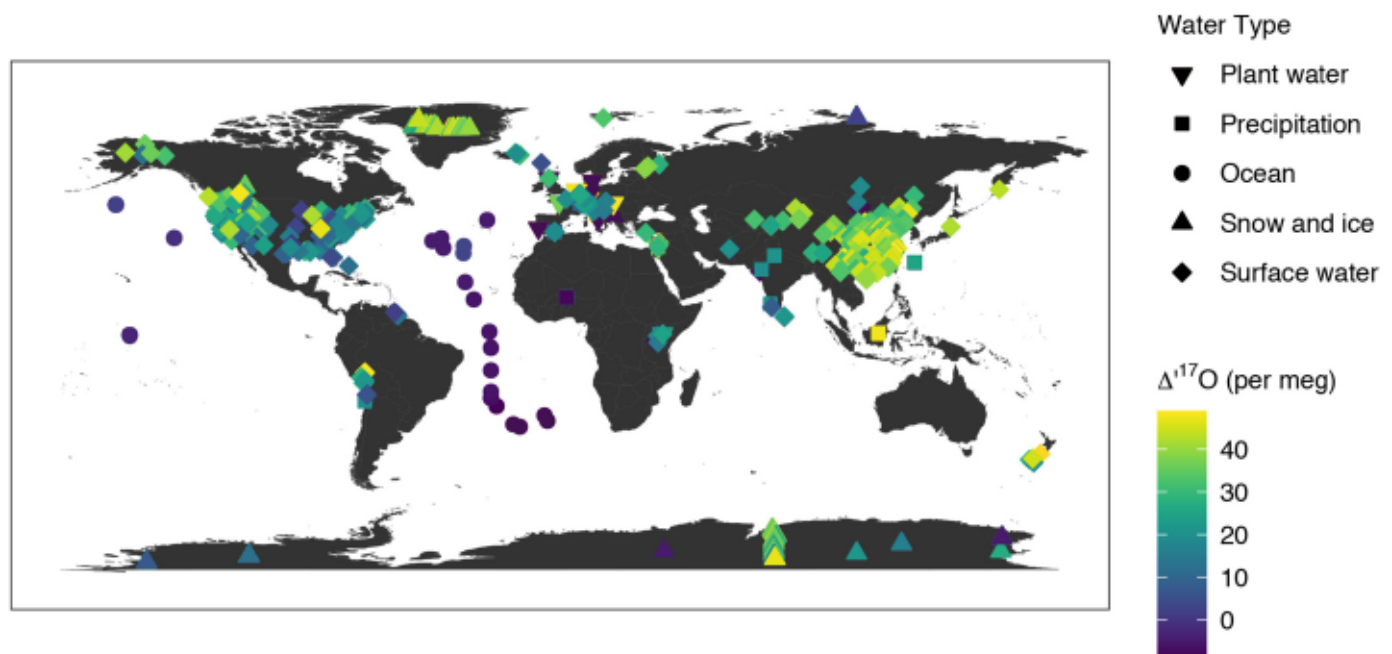


Fig. 6. Spatial variation of published (Table 2) meteoric water $\Delta^{17}\text{O}$ (per meg). Water types are differentiated by shape and $\Delta^{17}\text{O}$ values are differentiated by color. Note that the breaks on the color bar are spaced to highlight the $\Delta^{17}\text{O}$ variability between -10 and 40 per meg.

oxygen isotope meteoric water relationship.

The ^{18}O ^2H global meteoric water line was initially built from ~ 400 precipitation, river, and lake samples (Craig, 1961). Later, the meteoric water ^{18}O ^2H relationship was re-evaluated using amount-weighted and arithmetic mean monthly precipitation from a near-global distribution of IAEA/WMO sites (Dansgaard, 1964; Rozanski et al., 1993) and rivers from the United States (Kendall and Coplen, 2001). These re-evaluated global meteoric water lines have slightly higher slopes and intercepts, but are statistically indistinguishable from the original line defined by Craig (1961), indicating that the ^{18}O ^2H global meteoric water line is well characterized and represents global variation in ^{18}O and ^2H (Gat, 1996).

The triple oxygen global meteoric water line was first defined as (Luz and Barkan, 2010)

$$* \quad (6)$$

from GISP and SLAP (Barkan and Luz, 2005), 29 Vostok snow samples (Landais et al., 2008), and a set of 52 meteoric waters (precipitation, surface water, cave water, and snow) mostly from Europe and Asia (Luz and Barkan, 2010). The basic features of this line, an empirically determined slope and positive y-intercept, are similar to the oxygen-hydrogen global meteoric water line. However, the 2010 Luz and Barkan ^{18}O ^{17}O global meteoric water line was constructed with a large proportion of high latitude precipitation and samples (lakes, snow, and evaporated snow) with isotopic compositions that are not representative of average freshwater from the mid- and low-latitudes (Miller, 2018; Sharp et al., 2018). Building upon data that have been published since 2010, this review evaluates and updates the triple oxygen isotope global meteoric water line.

Following the approaches to build and evaluate the ^{18}O ^2H meteoric water relationship, the triple oxygen isotope meteoric water line should be defined from a regression through ^{18}O and ^{17}O of integrated monthly precipitation (Dansgaard, 1964; Rozanski et al., 1993) and/or flowing surface waters (rivers) (Kendall and Coplen, 2001). Precipitation data are preferable because they are generally unevaporated, but sample collection requires substantial effort and to date only eight studies have reported any precipitation ^{17}O data (Table 2). For now, river water is a reasonable alternative because it often represents the isotopic composition of amount-weighted seasonal precipitation (e.g., Kendall and Coplen, 2001). However, the isotopic composition of river water can be affected by post-precipitation processes such as evaporation or isotopic exchange with atmospheric vapor, so ultimately it will be important to re-evaluate the triple oxygen isotope meteoric water line with only integrated monthly precipitation data. This evaluation process will be especially important for ^{18}O and ^{17}O because one of the main applications of triple oxygen isotopes is to constrain evaporation.

The available triple oxygen isotope data (Table 2) from which we defined an updated meteoric water line include 1 river from north-western Switzerland (Affolter et al., 2015), 9 rivers from the western United States (Passey and Ji, 2019), 15 rivers from southern Spain (Gazquez et al., 2017), 17 rivers from the Sistan Basin in eastern Iran (Surma et al., 2015), 18 rivers from locations throughout Asia and Europe (Luz and Barkan, 2010), 57 rivers from the Pacific Northwest in the United States (Bershaw et al., 2020), and 84 rivers from our new surface water dataset (Section 4.1 and Supplement 1). Available precipitation data include amount-weighted monthly (Landais et al., 2010; Tian et al., 2018) and reported monthly (Gazquez et al., 2017; Uechi and Uemura, 2019) values. We do not include published data from individual precipitation samples because these data are not representative of monthly averages, nor do we include data from precipitation samples that were collected without any measure to prevent evaporation or for which the accuracy and precision of $\Delta^{17}\text{O}$ measurements were not explicitly presented.

The ^{18}O ^{17}O regression through the river and precipitation data

that are included in the updated meteoric water line is:

$$* \quad \% \quad (7)$$

Excluding rivers from very arid environments that may be affected by evaporation (Passey and Ji, 2019; Surma et al., 2015), the regression line is:

$$* \quad \% \quad (8)$$

The samples included in Eqs. (7) and (8) range from 20.5 to 9.4‰ in ^{18}O , and these regression lines are nearly indistinguishable from the best-fit line from a recent compilation of meteoric waters with ^{18}O values greater than 20‰ (^{17}O 0.52654* ^{18}O (0.00036) 0.014 (0.003); Sharp et al., 2018). In contrast, the regression line through samples with ^{18}O values less than 20‰,

$$* \quad \% \quad (9)$$

has a higher slope, higher intercept, and is similar to the 2010 global meteoric water line (Eq. (6)). Importantly, Eq. (9) is defined from every sample with a ^{18}O value less than 20‰ because currently there are only 12 samples (11 precipitation (Tian and Wang, 2019) and 1 river (this review)) that meet the criteria established by the ^{18}O ^2H global meteoric water line. Instead, more than 97% of the triple oxygen isotope samples with ^{18}O values less than 20‰ are from snow and ice from Antarctica or Greenland.

Differences between Eqs. (7) (9) suggests that triple oxygen isotopes do not fit a single, global meteoric water line. These differences may be associated with regional hydrologic processes as more than 95% of the samples included in Eq. (8) are from locations equatorward of 60° N and 60° S whereas more than 97% of the samples in Eq. (9) are from locations poleward of 60° N and 60° S. Alternatively, differences between Eqs. (8) and (9) may be related to water type, a sampling bias because most samples are clustered in small regions (Figs. 2 and 6), or insufficient data. For example, the Luz and Barkan (2010) triple oxygen isotope global meteoric water line was defined from all of the published precipitation, surface water, snow, and ice data in 2010, but does not fit all of the observations available today. Eqs. (7) (9) were defined from a subset of the published data in 2020 and better fit the observations available today, but may also become outdated with future work. For now, the available triple oxygen isotope data do not fit a single global meteoric water line. Future studies of flowing surface water and monthly precipitation are needed to further evaluate and properly establish this relationship. If triple oxygen isotopes do not fit a single global meteoric water line, that means the triple oxygen isotope system

Table 4

Observed (δ_{obs}) by water type. See Table 2 for references.

Sample subset	obs	standard error
All data	0.5273	0.00005
Luz and Barkan (2010)	0.5282	0.0003
Plant water	0.5188	0.0004
Precipitation	0.5273	0.0001
Ocean	0.5278	0.001
Snow and ice	0.5285	0.00006
Surface and subsurface	0.5261	0.0001

Table 5

Temperature dependence of equilibrium fractionation factors and Rayleigh.

Temperature (C)	^{18}O eq	^{17}O eq	Rayleigh
Calculation Explanation	Majoube, 1971	(^{18}O eq) ^{0.529}	(^{17}O eq 1)/(^{18}O eq 1)
40	1.00823	1.00435	0.5280
25	1.00937	1.00495	0.5278
0	1.01172	1.00618	0.5275
25	1.01483	1.00782	0.5272

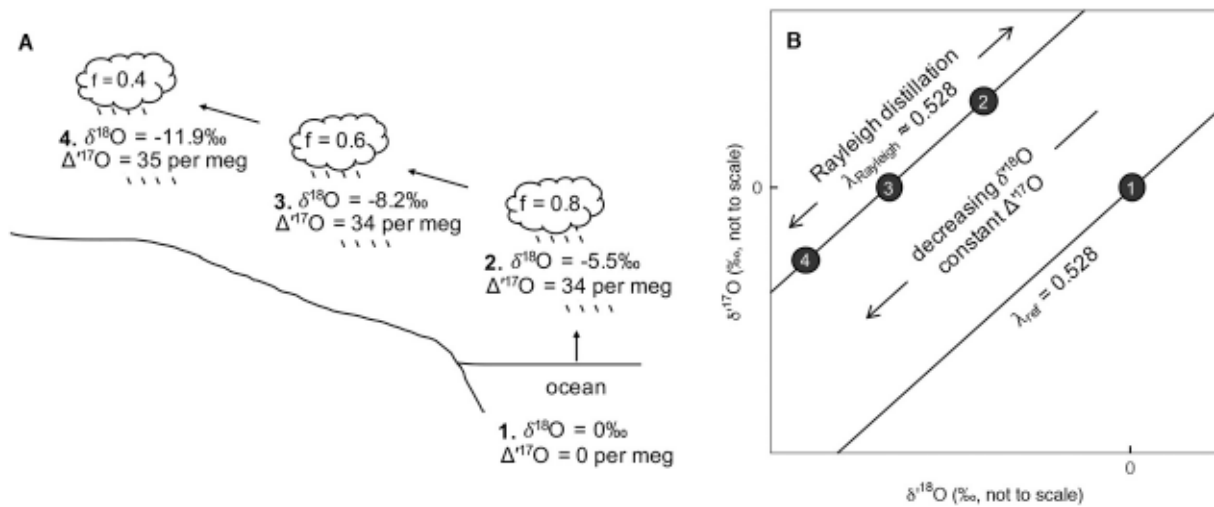


Fig. 7. Variation of liquid $\delta^{18}\text{O}$ and $\Delta^{17}\text{O}$ during Rayleigh distillation in (A) a schematic and (B) $\delta^{18}\text{O}$ – $\delta^{17}\text{O}$ isotope space. Water starts in the ocean (1), evaporates, and condenses, leaving air masses with (2) 80%, (3) 60%, and (4) 40% of the initial air mass remaining. In the schematic (A), f is the percentage of the initial air mass that remains after rainout. The isotopic composition of precipitation (steps 2–4) was calculated at 25°C and is assumed to be in isotopic equilibrium with the vapor shown in the middle row of Fig. 11. Because $\lambda_{\text{Rayleigh}}$ is approximately equal to λ_{ref} , $\Delta^{17}\text{O}$ is relatively insensitive to Rayleigh distillation.

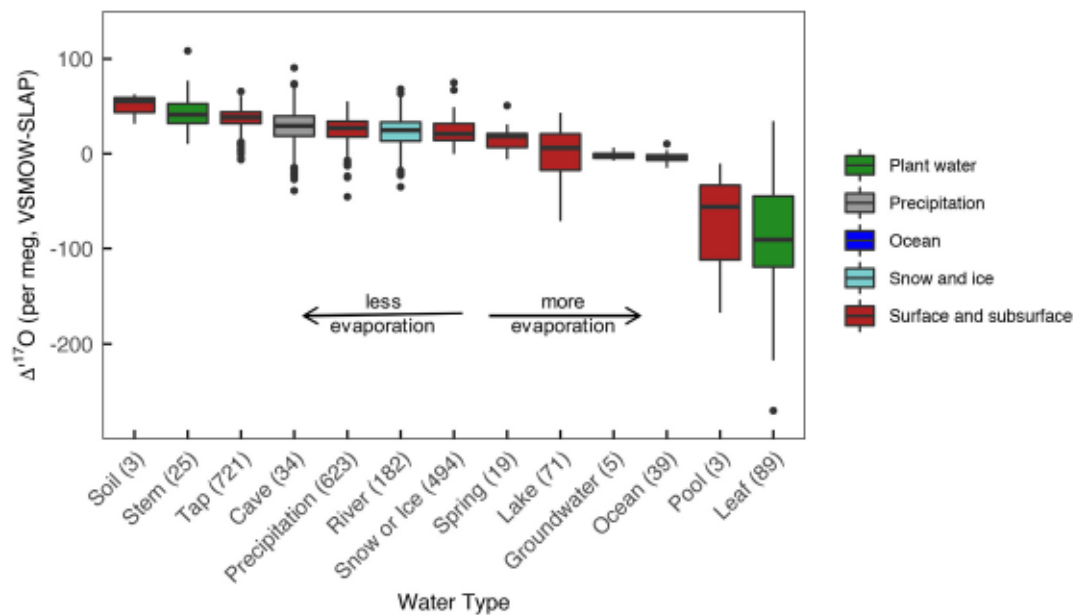


Fig. 8. Box and whisker plot of water $\Delta^{17}\text{O}$ values. Water types are listed individually, but are colored according to broader categories to give a sense of variation within groups. The numbers in parentheses indicate the total number of published observations for each water type and include the new surface water data reported in this review. In each box, the bolded line is the median $\Delta^{17}\text{O}$ value, the upper and lower hinge correspond to the 1st and 3rd quartiles, respectively, and the whiskers correspond to no more than 1.5 times the interquartile range (IQR, the variation between the 1st and 3rd quartiles). The individually plotted points fall outside the IQR. In general, more evaporated waters have lower $\Delta^{17}\text{O}$ values and less evaporated waters have higher $\Delta^{17}\text{O}$ values.

Table 6
Pearson correlation coefficient between $\Delta^{17}\text{O}$ – d -excess or $\delta^{18}\text{O}$.

Water type	$\Delta^{17}\text{O}$ – d -excess Correlation	$\Delta^{17}\text{O}$ – $\delta^{18}\text{O}$ Correlation
All Data	0.59	–0.17
Plant Water	0.95	–0.93
Lake	0.64	–0.79
Rain	0.21	–0.19
River	0.28	–0.09
Ocean	NA*	–0.03
Snow or Ice	–0.35	0.37

* There is no reported correlation between $\Delta^{17}\text{O}$ and d -excess for ocean water because only one sample (Bershaw et al., 2020) has reported $\delta^{18}\text{O}$, $\delta^{17}\text{O}$, and $\delta^2\text{H}$ of ocean water.

captures different parts of the hydrologic cycle that may not dominate equally across the globe.

5.2. Triple oxygen isotope reference slope

For much of the past decade it was assumed that all unevaporated meteoric water $\delta^{18}\text{O}$ and $\delta^{17}\text{O}$ values plotted on a single global meteoric water line with an observed slope (λ_{obs}) equal to the reference slope (λ_{ref}). With new observations, it is now known that meteoric water $\delta^{18}\text{O}$ and $\delta^{17}\text{O}$ values do not plot on a single water line, but instead that λ_{obs} can be quite variable (Table 4) and that the slope of a meteoric water line (λ_{mwl}) can vary among subsets of samples (Eqs. (7)–(9); Miller, 2018; Sharp et al., 2018). Variations among these values makes it critical

to understand differences between obs , mwl , and ref .

The observed slope (obs) is the slope through any particular dataset or group of samples. This value varies among studies, regions, and subsets of samples, and records hydrologic information because obs values are lower (closer to diff) when kinetic processes dominate isotopic compositions and higher (closer to eq) when equilibrium fractionation controls isotopic compositions (Table 4). The slope of a meteoric water line (mwl) defines an average or representative relationship among unevaporated waters. The ^{18}O ^{2}H model suggests that this value is constant globally, but triple oxygen isotope mwl values vary among subsets of samples or water types (Eqs. (7)–(9)). The reference slope (ref) is the reference frame from which $\Delta^{17}\text{O}$ is defined (Eq. (5)) and must remain constant. Typically, hydrologic triple oxygen isotope studies use a value of 0.528 for ref , and we recommend that authors continue to use this value. However, a value of 0.528 for ref is somewhat arbitrary, so it is important to understand where this value comes from and how it affects calculated $\Delta^{17}\text{O}$ values.

The value of ref was initially defined from a set of meteoric water ^{18}O and ^{17}O measurements made with electrolysis and continuous flow IRMS that fit a line with obs of 0.528 (Meijer and Li, 1998, obs 0.5281 ± 0.0015). This slope was later confirmed with a different set of water samples and higher precision dual inlet IRMS measurements (Luz and Barkan, 2010 obs 0.528 ± 0.0001), and defined as ref . That these obs values are closer to 0.529 (eq) than to 0.518 (diff) and are nearly identical to the ref value during Rayleigh distillation (Rayleigh, Table 5) indicates that most meteoric waters in these initial studies were more strongly affected by Rayleigh distillation than by kinetic fractionation.

Of course, the isotopic composition of meteoric water reflects more than just Rayleigh distillation, and observations over the last decade show that obs is not always equal to 0.528. When obs is equal to ref (e.g., during Rayleigh distillation), ^{18}O and ^{17}O fractionate along a line parallel to ref and $\Delta^{17}\text{O}$ values remain constant (Figs. 3a, 7, and 8a). When obs is less than ref , ^{18}O and $\Delta^{17}\text{O}$ are negatively correlated. The magnitude of this effect varies on a case-by-case basis and authors should carefully consider differences between obs and ref as a part of $\Delta^{17}\text{O}$ interpretations.

6. Hydrologic processes that affect $\Delta^{17}\text{O}$

The previous section focused on important distinctions among triple oxygen isotope slopes, but the magnitude of these variations is very small and ^{18}O ^{17}O compilations almost always appear exactly linear (Fig. 4c). Instead, triple oxygen isotope variations are commonly presented and interpreted in ^{18}O $\Delta^{17}\text{O}$ isotope space (for example, Fig. 3a–c). This space highlights mass-dependent deviations from the reference relationship (Farquhar and Thiemens, 2000; McKeegan and Leshin, 2001) and is a helpful way to simultaneously visualize isotopic compositions of ^{18}O (‰) and $\Delta^{17}\text{O}$ (per meg, where 1 per meg

0.001‰).

The ^{18}O versus $\Delta^{17}\text{O}$ isotope space is analogous to ^{18}O versus d-excess (Fig. 1). However, plots of ^{18}O versus d-excess are relatively uncommon because most hydrologically relevant deviations from the ^{18}O ^{2}H reference line are already visible in plots of ^{18}O versus ^{2}H . For example, the very evaporated plant waters in Fig. 4a clearly deviate from the rest of the less evaporated or unevaporated data. These deviations are visible in plots of ^{18}O versus ^{2}H because the difference between the reference slope (8) and kinetic slopes (typically ~4–6; Bowen et al., 2019; Gonfiantini et al., 2018) is the same or similar order of magnitude as ^{18}O and ^{2}H variations (typically a few to 10s of ‰). Similar deviations are not visible in the ^{18}O versus ^{17}O plot (Fig. 4c) because the difference between the reference slope (0.528) and kinetic slope (diff 0.518) is orders of magnitude smaller than variations of ^{18}O and ^{17}O (a few to 10s of ‰). Therefore, mass-dependent triple oxygen isotope variations are instead presented in ^{18}O $\Delta^{17}\text{O}$ isotope space.

6.1. Variability of $\Delta^{17}\text{O}$ in meteoric water

Average meteoric water $\Delta^{17}\text{O}$ is 20 to 30 per meg, but ranges from less than 250 per meg to greater than 100 per meg (Fig. 3b). Generally, more evaporated waters have lower $\Delta^{17}\text{O}$ values and less evaporated waters have higher $\Delta^{17}\text{O}$ values (Fig. 8). Among all published meteoric water data, $\Delta^{17}\text{O}$ is positively correlated with d-excess (r 0.59, Fig. 3e) and uncorrelated with ^{18}O (r 0.17, Fig. 3b), but these correlations vary substantially among water types (Table 6). For example, $\Delta^{17}\text{O}$ and d-excess of highly evaporated waters such as plant water and lakes are strongly positively correlated (r 0.95 and 0.64, respectively, Table 6) whereas $\Delta^{17}\text{O}$ and ^{18}O are strongly negatively correlated (r 0.93 and 0.79, respectively, Table 6). These plant water and lake correlations are so strong because both d-excess and $\Delta^{17}\text{O}$ are sensitive to relative humidity and vary as a function of kinetic fractionation. The slope between d-excess and $\Delta^{17}\text{O}$ is ~0.7 to 2.0 per meg ‰⁻¹ (e.g., Landais et al., 2010; Li et al., 2015), but the exact value varies as a function of relative humidity and fractionation factors (Barkan and Luz, 2007). Correlations from less evaporated waters such as precipitation and rivers are weaker between $\Delta^{17}\text{O}$ and d-excess (r 0.28 and 0.21, respectively, Table 6) or ^{18}O (r 0.19 and 0.09, respectively, Table 6). These weak correlations mean that processes other than evaporation must account for the $\Delta^{17}\text{O}$ variation of precipitation and river water.

Published meteoric water $\Delta^{17}\text{O}$ data are poorly suited for spatial analysis and there are no clear spatial trends in Fig. 6. In part this occurs because most $\Delta^{17}\text{O}$ observations are clustered in small regions and very few datasets systematically span latitudinal or elevational gradients (Figs. 2 and 6), but also because $\Delta^{17}\text{O}$ is primarily sensitive to kinetic fractionation and relatively insensitive to temperature effects and

Table 7
Processes and explanations of $\Delta^{17}\text{O}$ variation.

Process	$\Delta^{17}\text{O}$ Response	Magnitude of $\Delta^{17}\text{O}$ Response	Explanation
Evaporation from the ocean	increase	Typically ~ 20–30 per meg. Higher values with low humidity and/or low turbulence at the evaporating site.	eq vs. diff and diff less than ref
Condensation	increase	~ 10 per meg. Higher $\Delta^{17}\text{O}$ expected in colder conditions.	eq greater than ref
Recycling	increase	Typically ~ 20 per meg	diff less than ref
Stratospheric intrusions	increase	?	Addition of stratospheric water vapor
Post-condensation evaporation	decrease	Depends on stratospheric and tropospheric $\Delta^{17}\text{O}$ values Potentially ~ 200 per meg in plant water, typically no more than ~ 50–60 per meg in surface water	diff less than ref
Mixing	decrease	0 to ~ 100 per meg. Depends on the mixing fraction and initial ^{18}O and $\Delta^{17}\text{O}$ of the mixing waters	Non-linear response
Supersaturation	decrease	~ 10 to 30 per meg	diff less than ref
Rayleigh distillation	temperature dependent	10 per meg. Larger effect at lower temperatures.	Rayleigh ref
Convection	?	?	?

Rayleigh distillation (see Section 6.2.4 and Luz and Barkan, 2010). In this way, expectations of spatial $\Delta^{17}\text{O}$ variation are more similar to d-excess than to $\delta^{18}\text{O}$. Spatial $\Delta^{17}\text{O}$ patterns are also complicated because there is often more $\Delta^{17}\text{O}$ variation within a single study than between studies. For example, Li et al. (2017) link more than 50 per meg (~ 40 to -15 per meg) of $\Delta^{17}\text{O}$ variation to evapotranspiration and local relative humidity in central Kenya. However, a similar range of $\Delta^{17}\text{O}$ variability is related to summer sublimation in Antarctica (Pang et al., 2019) or relative humidity above remote moisture sources in southern Japan (Uechi and Uemura, 2019). Individually, each of these datasets tell a compelling story of local-to-regional hydrology; together, they do not paint a robust picture of large-scale spatial $\Delta^{17}\text{O}$ patterns.

Isotope-enabled climate models can fill some gaps that are missing from observations (e.g., Risi et al., 2013), and meteoric water $\Delta^{17}\text{O}$ values do tend to be lower in arid regions due to sub-cloud and surface evaporation and higher in regions where annual precipitation is dominated by cold-season rain or locations that receive a high degree of recycled moisture (see Section 6.2.3.1). Hydrologic mixing may also decrease $\Delta^{17}\text{O}$ values in regions where airmasses or other water bodies combine (Landais et al., 2010; Li et al., 2015; Risi et al., 2013). For example, lower tap water $\Delta^{17}\text{O}$ values in the central United States may result from atmospheric mixing of moisture that originated in the Pacific Ocean and the Gulf of Mexico (Li et al., 2015). Latitudinal $\Delta^{17}\text{O}$ gradients are observed in tap waters from the United States (Li et al., 2015) but not in China (Tian et al., 2019), although additional work is needed to understand this pattern (Fig. 6) because tap water $\Delta^{17}\text{O}$ values are complicated by non-local isotope signals.

Temporal $\Delta^{17}\text{O}$ patterns are also still relatively uncertain because only a few studies have focused on this type of variability (Table 2). Still, a seasonal pattern of mid-latitude precipitation $\Delta^{17}\text{O}$ is emerging, with lower values in the summer and higher values in the winter (Affolter et al., 2015; Li et al., 2015; Tian et al., 2018; Uechi and Uemura, 2019). This seasonal pattern may be related to variations in relative humidity and evaporative conditions above remote moisture sources (Tian et al., 2018; Uechi and Uemura, 2019). Condensation temperature may also play a role in seasonal $\Delta^{17}\text{O}$ variation (Table 5), but these effects are likely smaller than those related to relative humidity because $\Delta^{17}\text{O}$ is more sensitive to kinetic fractionation than to temperature.

6.2. Hydrologic processes that affect $\Delta^{17}\text{O}$

Most meteoric waters occupy a crowded region in $\delta^{18}\text{O}$ - $\Delta^{17}\text{O}$ isotope space, and many of the distinct patterns that differentiate plant

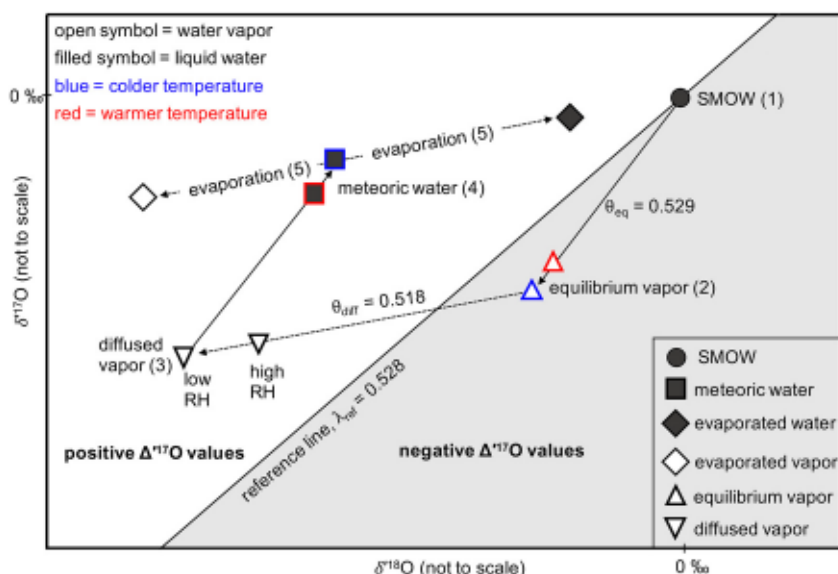


Fig. 9. Generalized pathway of $\delta^{18}\text{O}$ and $\delta^{17}\text{O}$ fractionation in the water cycle. In this $\delta^{18}\text{O}$ versus $\delta^{17}\text{O}$ isotope space, $\Delta^{17}\text{O}$ is defined as the deviation from the reference line. The white background indicates isotope spaces with positive $\Delta^{17}\text{O}$ values; the gray background indicates isotope spaces with negative $\Delta^{17}\text{O}$ values. Water at different points in the hydrologic cycle is differentiated with symbols and numbered 1-5 to show stepwise variation associated with evaporation and condensation. Beginning from the ocean (SMOW, 1), water evaporates into a saturated equilibrium layer (2), diffuses through the unsaturated atmosphere (3), condenses (4), and evaporates (5). Vapor is noted with open symbols; liquid is noted with filled symbols. The symbols do not indicate end points, but instead show points on a trajectory (marked with arrows) along which isotopic compositions can continue. Red (warmer) and blue (colder) outlines show the effects of temperature dependent fractionations. For clarity, values of λ_{ref} , θ_{eq} (solid line), and θ_{diff} (dotted line) are included. Additional details and a step-by-step description of $\delta^{18}\text{O}$ and $\delta^{17}\text{O}$ fractionations are shown in Fig. 10.

water and snow or ice (Fig. 3b) disappear among precipitation and surface waters (Fig. 3c). However, the $\Delta^{17}\text{O}$ values of precipitation and surface waters vary by more than 80 per meg, significantly greater than the precision of well-tuned $\Delta^{17}\text{O}$ measurements, and systematic trends exist within this cloud of isotope data that are related to hydrologic processes and well-known mass-dependent fractionations. The next sections describe the processes that drive this variation.

From a mechanistic point of view, $\Delta^{17}\text{O}$ variability arises from 1) changes in θ values (θ_{eq} versus θ_{diff}), 2) differences between the values of λ_{ref} and θ_{eq} or θ_{diff} , or 3) non-linear isotope responses that result from the logarithmic δ' notation (Table 7). Initial $\Delta^{17}\text{O}$ variation during evaporation from the ocean is well explained by the Craig and Gordon (1965) model, but phase changes and mixing following this initial evaporation can combine, compound, or negate each other and complicate $\Delta^{17}\text{O}$ data.

To simplify interpretations of $\Delta^{17}\text{O}$ data, we first use the theoretical framework of the Craig and Gordon (1965) model to explain triple oxygen isotope variation during initial evaporation and condensation (Section 6.2.1, Figs. 9 and 10) and then describe how distinct hydrologic processes can further affect $\Delta^{17}\text{O}$ (Table 7 and Sections 6.2.2 and 6.2.3). For beginning readers, these sections are an introduction to the types of questions that triple oxygen isotopes can help answer. For experienced researchers, these sections outline the theoretical framework, common isotopic models, and hydrologic processes that may explain $\Delta^{17}\text{O}$ observations. This focus on process is not intended to explain global or site-specific observations, but rather to provide a mechanistic understanding of meteoric water $\Delta^{17}\text{O}$ variability. Code to calculate isotopic variation during initial evaporation and condensation (Supplement 4), mixing (Supplement 5), and post-condensation evaporation (Supplement 6) is included to help readers understand triple oxygen isotope variation.

6.2.1. Why do most meteoric waters have positive $\Delta^{17}\text{O}$ values?

The Craig and Gordon (1965) model of evaporation explains why most meteoric waters have positive $\Delta^{17}\text{O}$ values. To understand this, we break the theoretical Craig and Gordon (1965) framework into step-by-step processes and show isotopic variation schematically (Fig. 9) and step-wise (Figs. 10 and 11) as water evaporates from the ocean and then condenses. This section focuses on $\delta^{17}\text{O}$, $\delta^{18}\text{O}$, and $\Delta^{17}\text{O}$; $\delta^{18}\text{O}$, $\delta^2\text{H}$, and d-excess are included in Figs. 10 and 11 to highlight similarities between the $\delta^{18}\text{O}$ - $\delta^{17}\text{O}$ and $\delta^{18}\text{O}$ - $\delta^2\text{H}$ isotope systems. Arrows, color, and bolding in Figs. 9 and 10 highlight step-wise isotopic variation. The symbols, color (red versus blue), and bolding (bold versus nonbold) are the same in Figs. 9 and 10. In these figures, color differentiates

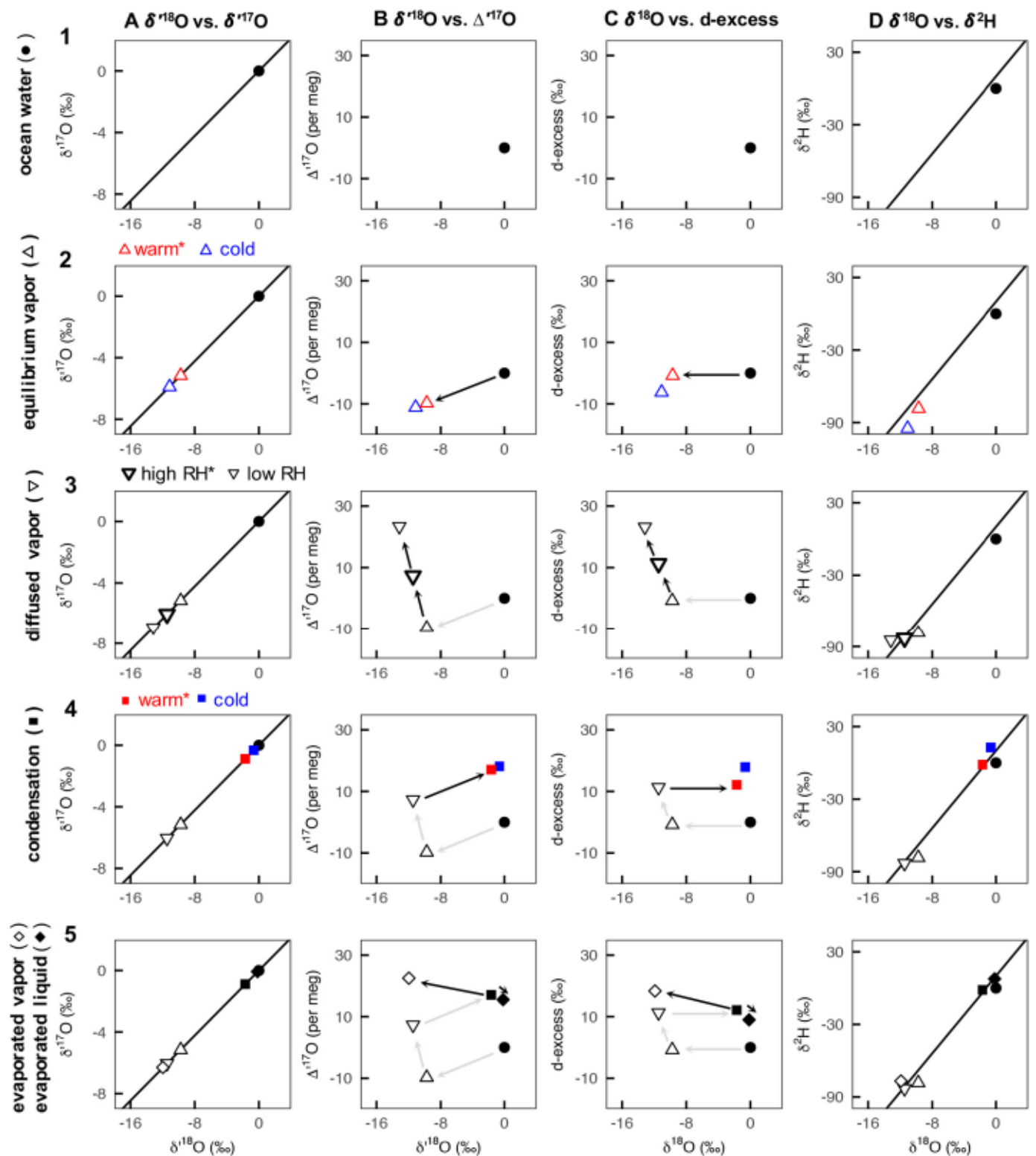


Fig. 10. Step-wise variation of $\delta^{17}\text{O}$, $\delta^{18}\text{O}$, $\delta^2\text{H}$, $\Delta^{17}\text{O}$, and d-excess as water evaporates and condenses in a closed system. Isotopic variation is shown between $\delta^{18}\text{O}$ and $\delta^{17}\text{O}$ (column A), $\delta^{18}\text{O}$ and $\Delta^{17}\text{O}$ (column B), $\delta^{18}\text{O}$ and d-excess (column C), and $\delta^{18}\text{O}$ and $\delta^2\text{H}$ (column D). The solid black lines in columns (A) and (D) show the triple oxygen and oxygen-hydrogen reference relationship, respectively. In each column, water begins in the ocean (row 1), evaporates into a saturated layer (row 2), diffuses through an unsaturated atmosphere (row 3), condenses to meteoric water (row 4), and evaporates (row 5). In row 4, we assume the isotopic composition of precipitation is equal to that of surface water. The isotopic compositions of evaporated vapor and remaining liquid were calculated assuming pan evaporation at 16°C and 10% evaporation. In all panels, vapor is shown with open symbols and liquid is shown with filled symbols. In columns B and C, black arrows show the isotopic variation associated with each row; gray arrows are included to show the ‘trajectory’ of isotope variability. Fractionation associated with equilibrium evaporation (row 2), atmospheric vapor diffusion (row 3), and condensation (row 4) are shown under different temperature and humidity scenarios with color and bolded symbols. When multiple scenarios are included, the star (*) notes which scenario is used in subsequent calculations (rows).

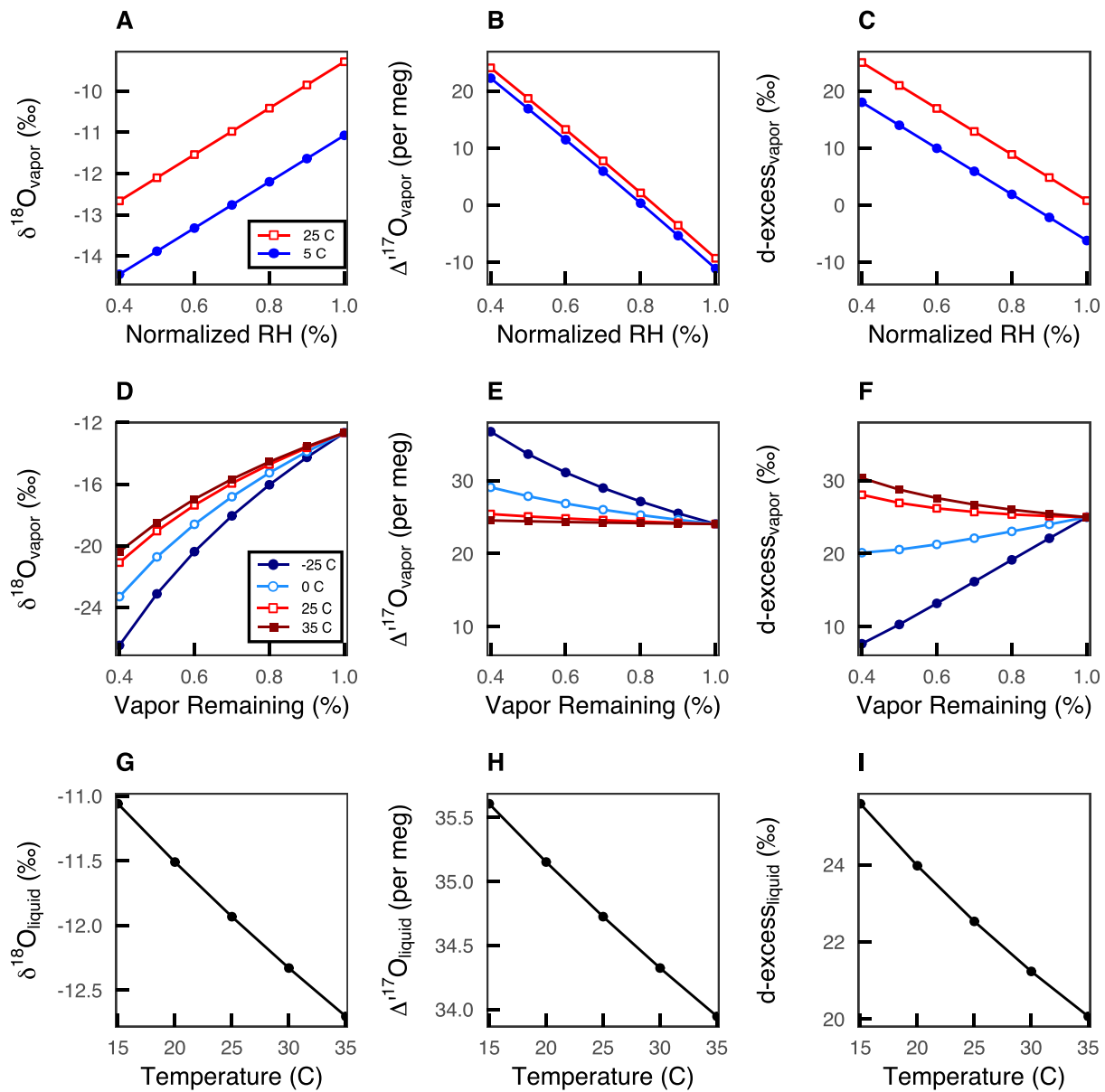


Fig. 11. Isotope variations of ^{18}O (A, D, G,), ^{17}O (B, E, H), and d-excess (C, F, I) during evaporation from the ocean and subsequent Rayleigh distillation. Row 1 (A, B, C) shows the sensitivity of evaporated vapor to temperature and relative humidity. Rows 2 (D, E, F) and 3 (G, H, I) show the temperature sensitivity of remaining vapor and condensed liquid, respectively. Fractionation under each temperature scenario is independent and does not represent a ‘trajectory’ from ocean water to precipitation. The final (RH = 0.4) 25 C water vapor from the top row is the starting vapor in the middle row. The final (RH = 0.4) 0 C vapor in the middle row is in isotopic equilibrium with the liquid in the bottom row. Note the different y-axes in each row.

temperature and bolding shows the sensitivity of isotopic compositions to relative humidity. Black arrows in Fig. 10 show the isotopic variation associated with each step, and gray arrows give a sense of the isotopic ‘trajectory’.

First, beginning from the ocean (Figs. 9 and 10, row 1), equilibrium isotope exchange (Fig. 10, row 2) occurs between water vapor (open upward-facing triangles) and liquid water (solid black circles) in a saturated layer near the evaporating surface. Because the value of α_{eq} (0.529) is greater than that of α_{ref} (0.528), ^{18}O and ^{17}O of the vapor fall below the reference line and $\Delta^{17}\text{O}$ is slightly negative (–9 per meg and –11 per meg at 25 C and 5 C, respectively, Figs. 9 and 10, panel 2b). The difference between the red (warmer) and blue (colder) open upward-facing triangles is very small within a typical temperature range (~0–30 C) because the value of α_{eq} is relatively insensitive to temperature (Barkan and Luz, 2005) and is similar to the value of α_{ref} .

Second, during diffusion through the unsaturated atmosphere

(Fig. 10, row 3), $\Delta^{17}\text{O}$ values of atmospheric vapor (open downward-facing triangles) increase because the value of α_{diff} (0.518) is less than the value of α_{ref} (Figs. 9 and 10, panel 3b). The magnitude of this kinetic effect is negatively correlated with turbulence above the saturated layer and sensitive to the relative humidity at the site of evaporation (Barkan and Luz, 2007; Criss, 1999; Merlivat, 1978; Uemura et al., 2010). The sensitivity of $\Delta^{17}\text{O}$ to relative humidity is labeled in Fig. 9 and shown with bolded (higher relative humidity) or nonbolded (lower relative humidity) symbols in the 3rd row of Fig. 10. When relative humidity is higher, kinetic fractionation is smaller and vapor $\Delta^{17}\text{O}$ values remain closer to zero. When relative humidity is lower, vapor $\Delta^{17}\text{O}$ values are higher (Figs. 9 and 10, panel 3b).

Third, equilibrium condensation (Fig. 10, row 4) proceeds along a slope (α_{eq} = 0.529) that is greater than the value of α_{ref} . This fractionation increases the $\Delta^{17}\text{O}$ value of the more condensed phase (precipitation, solid squares in Figs. 9 and 10, panel 4b) and decreases the $\Delta^{17}\text{O}$

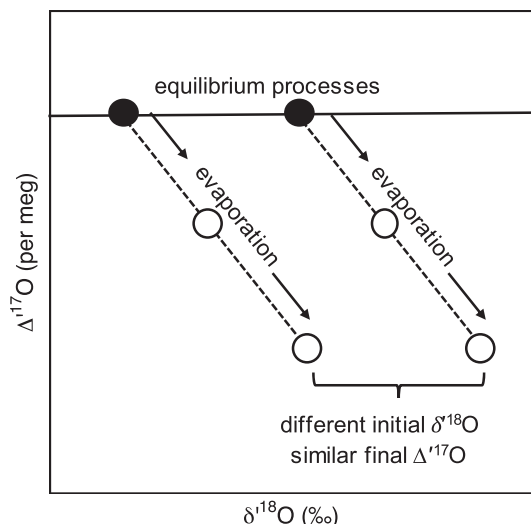


Fig. 12. Schematic of ^{18}O versus ^{17}O based on isotope mass balance models of steady-state evaporation. During evaporation, the ^{17}O response is independent of initial ^{18}O composition.

value of the less condensed phase (remaining vapor, Fig. 11e). Precipitation and vapor $\Delta^{17}\text{O}$ values are slightly sensitive to temperature during condensation (compare the red and blue squares in Figs. 9 and 10 and variations in Fig. 11e) because equilibrium fractionation is larger at lower temperatures than at higher temperatures (Fig. 9; 10, panel 4b; and 11e) (Horita and Wesolowski, 1994; Majoube, 1971). The increase in precipitation $\Delta^{17}\text{O}$ associated with equilibrium condensation is typically smaller than kinetic effects during diffusion because the value of α_{ref} is closer to the value of α_{eq} than the value of α_{diff} .

Fourth, post-condensation evaporation (Fig. 10, row 5) increases vapor (open diamonds) $\Delta^{17}\text{O}$ values and decreases the $\Delta^{17}\text{O}$ values of the remaining liquid (solid diamonds) because the value of α_{diff} is less than the value of α_{ref} (Figs. 9 and 10, panel 5b). This kinetic fractionation explains why some very evaporated waters such as plant waters and lakes (Figs. 3b and 8) have negative $\Delta^{17}\text{O}$ values.

6.2.2. Hydrologic processes that decrease $\Delta^{17}\text{O}$

6.2.2.1. Evaporative effects on remaining water. Evaporation leaves the remaining water body with higher ^{18}O and ^{17}O compositions (Gat, 1996; Gonfiantini et al., 2018) and a lower $\Delta^{17}\text{O}$ value because the value of α_{diff} is less than the value of α_{ref} (Figs. 9 and 10). These effects are most pronounced in leaf waters, lakes, and some slow-moving rivers

(Fig. 3b; Cernusak et al., 2016; Landais et al., 2006; Li et al., 2017). This fractionation is independent of initial ^{18}O , such that low $\Delta^{17}\text{O}$ values do not require high ^{18}O and vice versa (Fig. 12).

Evaporation occurs in the hydrosphere under steady-state (constant water levels) or non-steady-state (progressive water loss) conditions. The isotopic composition of remaining water in both of these scenarios is predicted by well-established models that apply to ^{18}O , ^{17}O , and ^2H (Criss, 1999; Gazquez et al., 2018; Passey and Ji, 2019; Surma et al., 2018). First, steady-state evaporation occurs in simple flow-through or closed-basin systems where the volume of inflowing water is equal to the volume of water loss via evaporation, outflow, and/or groundwater seepage. In this scenario, the isotopic composition of the remaining water is:

$$\dots \quad (10)$$

where α_{eq} is the temperature dependent equilibrium fractionation factor (Barkan and Luz, 2005; Horita and Wesolowski, 1994; Majoube, 1971), α_{diff} is the kinetic fractionation factor, h is the relative humidity normalized to the temperature of the evaporating surface, X_E is the volumetric ratio of water lost to evaporation relative to inflowing water, and R_i , R_A , and R_W are the isotope ratios of inflowing water, atmospheric water vapor, and remaining evaporated water, respectively. Importantly, this model assumes that the isotopic composition of the evaporating body is well mixed and that inflowing water is isotopically uniform and unevaporated, which is not always the case (e.g., Surma et al., 2018; Surma et al., 2015). Second, non-steady-state evaporation occurs in isolated water bodies that evaporate to dryness. The isotopic composition of the water body during this ‘pan evaporation is (Criss, 1999; Passey and Ji, 2019; Surma et al., 2018):

$$\dots \quad (11)$$

where f is the fraction of water remaining, R_W is the isotope ratio of the evaporating body, R_{Wi} is the isotope ratio of the initial water, R_{Wss} is the predicted final steady-state isotope ratio, and the exponent u relates equilibrium and kinetic fractionation factors by the relative humidity (h), where u is:

$$\dots \quad (12)$$

and R_{Wss} is:

$$\dots \quad (13)$$

Observations and modeling show that the isotopic effects of

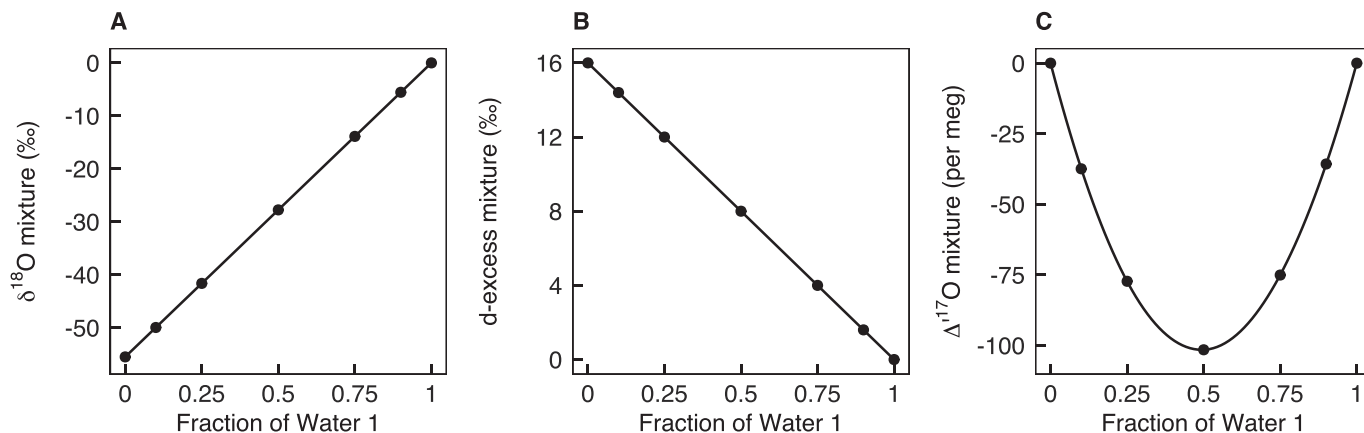


Fig. 13. Variations of (A) ^{18}O , (B) d-excess, and (C) ^{17}O values when mixing VSMOW (water 1) and SLAP (water 2). ^{18}O and d-excess vary linearly with mixing. ^{17}O responds nonlinearly to mixing because it is defined with δ notation.

evaporation are greatest when relative humidity is low and/or when values of δ_{diff} or X_E are high (Criss, 1999; Gazquez et al., 2018; Passey and Ji, 2019; Surma et al., 2018), although additional work is needed to clarify the role of turbulence at the evaporating site and to constrain the values of δ_{diff} and X_E (Passey and Ji, 2019).

6.2.2.2. Mixing. Due to the logarithmic notation used in the definition of $\Delta^{17}\text{O}$, mixing water bodies with different ^{18}O compositions decreases $\Delta^{17}\text{O}$ (Fig. 13c; Luz and Barkan, 2010; Matsuhisa et al., 1978). This phenomenon is most pronounced when $\Delta^{17}\text{O}$ of the mixed water bodies are identical and ^{18}O are very different. The ^{18}O and d-excess responses to mixing are a linear function of the fraction of each mixed water (Fig. 13a and b) because ^{18}O and d-excess are defined with notation (not logarithmic notation). Isotopic effects of mixing also affect analytical systems as gases move through prep lines and isotope analyzers (see Section 7.2.6 for additional details). Code in Supplement 5 is provided so researchers can explore the isotopic effects of mixing in natural and analytical settings.

6.2.2.3. Supersaturation. Kinetic effects during condensation under very cold (~ 20 C) supersaturated conditions cause low $\Delta^{17}\text{O}$ values in snow and ice (Angert et al., 2004; Jouzel and Merlivat, 1984; Landais et al., 2012a, 2012b; Landais et al., 2008; Pang et al., 2019; Pang et al., 2015; Risi et al., 2010; Schoenemann et al., 2014; Schoenemann and Steig, 2016; Winkler et al., 2012) and a pattern of downward tailing $\Delta^{17}\text{O}$ at very low (^{18}O 30‰) isotopic compositions (Fig. 3b). Supersaturation is common in high latitude and polar regions and develops when the saturation vapor pressure of a condensing surface is less than the vapor pressure surrounding a water droplet or ice crystal (Schoenemann et al., 2014). Under these conditions, a strong vapor pressure gradient develops between water vapor and the condensing surface. Water vapor must diffuse across this gradient to condense, a process that causes kinetic fractionation and lowers $\Delta^{17}\text{O}$ values of the condensate. Although equilibrium effects during condensation (Section 6.2.1) and moisture recycling in Antarctica (Pang et al., 2019) generally increase $\Delta^{17}\text{O}$, low $\Delta^{17}\text{O}$ values observed in polar regions (Fig. 3b) suggest that strong kinetic effects dominate under very cold supersaturated conditions (Angert et al., 2004; Jouzel and Merlivat, 1984; Landais et al., 2012a).

6.2.3. Hydrologic processes that increase $\Delta^{17}\text{O}$

6.2.3.1. Moisture recycling. Moisture recycling increases $\Delta^{17}\text{O}$ of evaporated vapor and subsequent precipitation because the value of δ_{diff} is less than the value of δ_{ref} (Figs. 9 and 10). Maintaining isotopic and mass balance and following the logic that describes fractionation of remaining water during evaporation (Section 6.2.2.1), evaporated vapor has lower ^{18}O , lower ^{17}O , and higher $\Delta^{17}\text{O}$ than the initial water body from which it evaporated. The $\Delta^{17}\text{O}$ of this vapor is inversely related to the relative humidity at the site of evaporation, with lower relative humidity resulting in higher vapor $\Delta^{17}\text{O}$ values (Figs. 9 and 10). Condensation of this recycled moisture further increases $\Delta^{17}\text{O}$ (Figs. 9 and 10). d-excess also increases with moisture recycling (Aemisegger et al., 2014; Salati et al., 1979; Tian et al., 2019), so $\Delta^{17}\text{O}$ and d-excess of evaporated vapor are positively correlated (Figs. 3e and 10, panels 5b and 5c).

6.2.3.2. Stratospheric intrusions. Stratospheric water vapor undergoes non-mass-dependent fractionation and has extremely high (greater than 1,000 per meg) $\Delta^{17}\text{O}$ values (Miller, 2018; Winkler et al., 2012) that may contribute to surface water fluxes. Stratospheric intrusions are possible during the Antarctic winter when the tropopause is low (Franz et al., 2005; Roscoe et al., 2004), but are generally considered negligible in most hydrologic triple oxygen isotope studies (e.g., Landais et al., 2008; Luz and Barkan, 2010) and are not evident in Fig. 3.

6.2.4. Hydrologic processes with little effect on $\Delta^{17}\text{O}$

6.2.4.1. Rayleigh distillation. Rayleigh distillation explains many of the spatial patterns observed in meteoric water ^{18}O , ^{17}O , and ^2H (Gat, 1996; Risi et al., 2013), but has little effect on $\Delta^{17}\text{O}$ (Fig. 7) because δ_{Rayleigh} (Table 5) is nearly identical to δ_{ref} (0.528) (Fig. 7b, Luz and Barkan, 2010). In other words, during Rayleigh distillation ^{18}O and ^{17}O vary along a line that is nearly parallel to δ_{ref} , so $\Delta^{17}\text{O}$ remains essentially constant. A slight temperature dependence of δ_{Rayleigh} (0.5278 at 25 C, 0.5272 at 25 C; Table 5) and can increase (decrease) the $\Delta^{17}\text{O}$ value of vapor (condensate) by a few per meg when δ_{Rayleigh} is less than δ_{ref} (Fig. 11), but this variation is generally smaller than analytical precision (approximately 10 per meg). The temperature

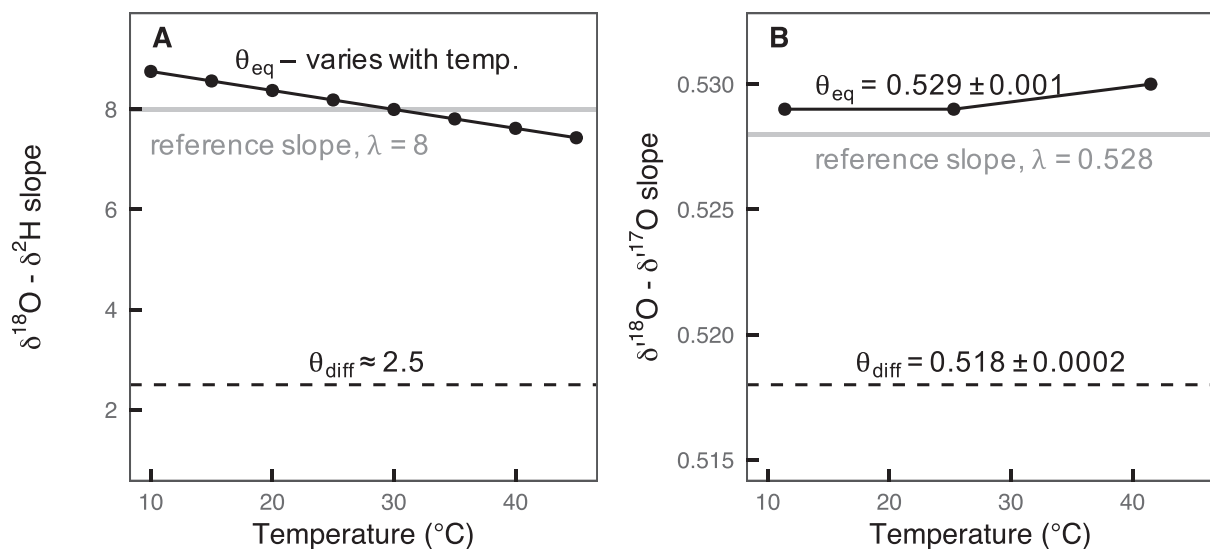


Fig. 14. Temperature dependence of the slopes in (A) ^{18}O – ^2H and (B) ^{18}O – ^{17}O isotope systems. Slopes are shown for equilibrium fractionation (θ_{eq} , solid black line), the diffusion of water vapor through the air (θ_{diff} , dashed black line), and the meteoric water reference relationship (solid gray line). The reference slopes are well-established (Craig, 1961 and Luz and Barkan, 2010, respectively) and do not vary with temperature. Similarly, θ_{diff} values are independent of temperature (Barkan and Luz, 2007). The θ_{diff} value associated with the ^{18}O – ^2H relationship is generally between ~ 2.5 and 8 (Gonfiantini et al., 2018). The triple oxygen (^{18}O – ^{17}O) θ_{eq} value is insensitive to temperature (Barkan and Luz, 2005); the oxygen–hydrogen (^{18}O – ^2H) θ_{eq} value varies slightly with temperature. These different θ_{eq} temperature sensitivities result in a slight temperature dependence in d-excess but little temperature dependent variation in ^{17}O .

sensitivity of α_{Rayleigh} arises from the equilibrium fractionation factors (values) for ^{18}O and ^{17}O (Barkan and Luz, 2005; Luz and Barkan, 2010; Majoube, 1971) because

$$\left(\frac{\alpha_{\text{Rayleigh}}}{\alpha_{\text{ref}}} \right) \quad (14)$$

As a result, values of α_{Rayleigh} are slightly higher at warmer temperatures and slightly lower at cooler temperatures (Table 5). At very warm temperatures ($> 35\text{ }^\circ\text{C}$), α_{Rayleigh} is almost identical to α_{ref} and $\Delta^{17}\text{O}$ is indeed invariant during Rayleigh distillation (Table 5, Fig. 11).

6.2.4.2. Temperature sensitivity of $\Delta^{17}\text{O}$. Theoretical calculations and laboratory experiments show that $\Delta^{17}\text{O}$ is relatively insensitive to temperature, and far less sensitive to temperature than d-excess (Figs. 10, 11, and 14b; Barkan and Luz, 2005; Cao and Liu, 2011). These different temperature sensitivities occur because the triple oxygen liquid-vapor α_{eq} value is independent of temperature (Fig. 14b; Barkan and Luz, 2005; Cao and Liu, 2011), whereas the oxygen-hydrogen liquid-vapor α_{eq} value varies slightly with temperature (Fig. 14a; Horita and Wesolowski, 1994; Majoube, 1971). For both the triple oxygen and oxygen-hydrogen systems, the α_{eq} value is defined as:

$$\alpha_{\text{eq}} = \frac{R_{\text{vapor}}}{R_{\text{liquid}}} \quad (15)$$

where α_{eq} is the temperature dependent equilibrium liquid-vapor fractionation factor for A ($^2\text{H}/^1\text{H}$ or $^{17}\text{O}/^{16}\text{O}$) and B ($^{18}\text{O}/^{16}\text{O}$). The triple oxygen α_{eq} value is nearly invariant (0.529, Fig. 14b) because $^{17}\text{O}/^{16}\text{O}$ and $^{18}\text{O}/^{16}\text{O}$ are subject to the same temperature effects; the oxygen-hydrogen α_{eq} value (~ 8 , Fig. 14a) varies slightly with temperature because $^2\text{H}/^1\text{H}$ fractionation is governed by a different temperature dependent relationship than $^{18}\text{O}/^{16}\text{O}$ fractionation (Horita and Wesolowski, 1994; Majoube, 1971).

The different temperature sensitivities of $\Delta^{17}\text{O}$ and d-excess are most noticeable at low temperatures (low ^{18}O values, compare Fig. 3b and d) and can provide complementary information to decouple the isotopic effects of temperature, relative humidity, and supersaturation on meteoric waters (Landais et al., 2012a, 2012b; Landais et al., 2008; Uemura et al., 2010; Winkler et al., 2012).

7. Analytical methods and considerations

7.1. Analytical methods to measure water $\Delta^{17}\text{O}$

Triple oxygen isotope ratios are measured with dual inlet isotope ratio mass spectrometry or laser absorption spectrometry (Table 8). With careful analysis, both methods can achieve high quality $^{17}\text{O}/^{16}\text{O}$ measurements and similar (~ 10 per meg) precision for the $\Delta^{17}\text{O}$ parameter. Typically, triple oxygen isotope data are measured in analytical sessions and data corrections (VSMOW-SLAP normalization, drift corrections, etc.) are applied over a full session (Thompson, 2012; Werner and Brand, 2001). For IRMS systems, an analytical session is defined for each reactor (~ 200 injections) and lasts approximately 2–4

weeks of near-constant analysis; for laser-based systems, an analytical session is typically defined as a batch or tray of samples or a 'calibration window' as in Schauer et al. (2016) that can span a few days to a few months.

7.1.1. Dual inlet isotope ratio mass spectrometry

The IRMS cobalt(III) fluoride method was first described by Baker et al. (2002) and was later modified by Barkan and Luz (2005) to improve the precision of ^{17}O and ^{18}O measurements. In this process, water is fluorinated to convert liquid water to oxygen gas:

$$(16)$$

Following fluorination, O_2 gas passes through a series of traps and molecular sieves to remove reaction byproducts and capture the purified sample. Triple oxygen isotope ratios are measured on O_2 gas using Thermo-Finnigan Delta Plus (e.g., Luz and Barkan, 2010), Thermo-Finnigan 253 (e.g., Schoenemann et al., 2014), or Nu Perspective (this study) mass spectrometers. In total, a single measurement takes ~ 3 hours and samples are typically analyzed twice. IRMS methods and an analytical workflow from our lab at the University of Michigan are described in Section 8.2.

7.1.2. Laser absorption spectrometry

Because the fluorination and IRMS methods are complex and require significant laboratory infrastructure (see Section 8.2), there is interest in using cavity ring-down spectroscopy (Picarro Inc.) or cavity-enhanced laser absorption (Los Gatos Research, LGR) to measure triple oxygen isotope ratios. These laser absorption spectrometers can achieve similar $\Delta^{17}\text{O}$ precision as IRMS techniques, have a smaller laboratory footprint, are cheaper and more portable than mass spectrometers, and simultaneously measure ^{18}O , ^{17}O , and ^2H (Berman et al., 2013; Schauer et al., 2016; Steig et al., 2014). Laser absorption spectrometry may also be faster than the IRMS method because laser-based analyzers do not require complex sample conversion from liquid water to gaseous O_2 and the absorption analysis only takes a few minutes. However, high-quality laser absorption isotope data require long integration times (Schauer et al., 2016; Steig et al., 2014) or many injections of the same sample, which can cumulatively take longer than a single IRMS analysis (Berman et al., 2013), and additional work is needed to directly compare ^{18}O , ^{17}O , and $\Delta^{17}\text{O}$ data from laser-based and IRMS systems. An example of the workflow required to achieve ~ 10 per meg $\Delta^{17}\text{O}$ precision on a Picarro water isotope analyzer is described in Schauer et al. (2016).

7.2. Analytical recommendations and best practices

7.2.1. VSMOW-SLAP normalization

We recommend that triple oxygen isotope compositions be normalized to the VSMOW-SLAP scale following the approach described by Schoenemann et al. (2013). We provide code (Supplement 7) and an example data file (Supplement 8) to show how to do this normalization. This normalization technique improves the accuracy of isotope measurements, simplifies inter-lab data comparisons (Brand and Coplen, 2001; Coplen, 1988; Gonfiantini, 1978; Meijer et al., 2000; Paul et al.,

Table 8
Water triple oxygen isotope analysis methods.

	IRMS	Picarro	Los Gatos Research (LGR)
Analysis method	Dual-inlet isotope ratio mass spectrometry (IRMS)	Cavity ring-down spectroscopy (CRDS, laser-based)	Cavity-enhanced laser absorption spectroscopy
Instrument	Various (Delta Plus, MAT 253, Nu Perspective)	L2140-i	Triple Water Isotope Analyzer (TWIA)
Sample preparation	CoF_3 reaction	$\text{H}_2\text{O}_{(\text{l})}$ $\text{H}_2\text{O}_{(\text{g})}$	$\text{H}_2\text{O}_{(\text{l})}$ $\text{H}_2\text{O}_{(\text{g})}$
Analyte	O_2 gas	Water vapor	Water vapor
Analysis time	2 to 3 hours	1.5 to 3 hours	1 hour to 7 hours
$\Delta^{17}\text{O}$ precision	~ 10 per meg	8 per meg	~ 10 per meg
Lab footprint	10s m^2	1-2 m^2	1-2 m^2
Method development	Barkan and Luz, 2005	Steig et al., 2014; Schauer et al., 2016	Berman et al., 2013

Table 9
Isotopic composition of common standards and reference waters.

	^{18}O (‰)	^{17}O (‰)	^2H (‰)	$\Delta^{17}\text{O}$ (per meg)
VSMOW ^a , VSMOW2 ^b	0	0	0	0
SLAP ^a , SLAP2 ^b	55.5	29.6968 ^c	428.0	0
GISP	24.78 0.09 ^e	13.16 0.05 ^c	189.7 1.0 ^e	22 11 ^c
		13.12 0.05 ^d		23 10 ^d
		13.5 0.3 ^f		24 12 ^f
USGS 45	2.238 0.011 ^e	1.19 0.3 ^d	10.3 0.4 ^e	12 1 ^d
		1.1 0.3 ^f		13 7 ^f
USGS 46	29.80 0.03 ^e	15.85 0.02 ^d	235.8 0.7 ^e	20 2 ^d
		15.7 0.2 ^f		19 11 ^f
USGS 47	19.80 0.02 ^e	10.47 0.02 ^d	150.2 0.5 ^e	40 1 ^d
		10.4 0.4 ^f		32 9 ^f
USGS 48	2.224 0.012 ^e	1.15 0.01 ^d	2.0 0.4 ^e	26 3 ^d
		1.1 0.2 ^f		31 6 ^f
USGS 49	50.55 0.04 ^e	27.8 0.5 ^f	394.7 0.4 ^e	13 8 ^f
USGS 50	4.95 0.02 ^e	2.7 0.2 ^f	32.8 0.4 ^e	10 7 ^f

Notes: All isotopic data are normalized to the VSMOW-SLAP scale.

^a Gonfiantini, 1978; Barkan and Luz, 2005.

^b Lin et al., 2010.

^c Schoenemann et al., 2013.

^d Berman et al., 2013 (isotopic data are weighted by the inverse of precision; uncertainties are the averages of three experimental methods weighted by the number of measurements).

^e USGS Reports of Stable Isotopic Composition Reference Materials (uncertainty is the 95% confidence interval).

^f This study (uncertainty is one unweighted standard deviation). The $\Delta^{17}\text{O}$ of USGS47 reported in this study is substantially lower than the value from Berman et al. (2013). Our measured ^{18}O and ^{17}O values are nearly identical to the accepted (USGS) or previously published (Berman et al., 2013) values, and we do not have a compelling analytical explanation for this one low $\Delta^{17}\text{O}$ value.

2007; Schoenemann et al., 2013), and corrects for analytical inconsistencies such as pressure-baseline offsets (Yeung et al., 2018).

At a minimum, VSMOW and SLAP (or VSMOW2 and SLAP2, which are isotopically indistinguishable from VSMOW and SLAP (Lin et al., 2010)), should be measured the beginning and end of every analytical session. Ideally, VSMOW or VSMOW2 and SLAP or SLAP2 should also be analyzed within each session because instrument nonlinearities can evolve through time. We recommend that the value of $^{17}\text{O}_{\text{SLAP}}$ (29.6968‰) be calculated directly from the defined values of $^{18}\text{O}_{\text{SLAP}}$ (55.5‰), $\Delta^{17}\text{O}_{\text{SLAP}}$ (0.00‰), and α_{ref} (0.528) (Gonfiantini, 1978; Schoenemann et al., 2013) because this approach results in excellent inter-lab $\Delta^{17}\text{O}$ reproducibility and mathematically is the same approach that most labs already use to correct ^{18}O data (Berman et al., 2013; Kaiser, 2009; Schoenemann et al., 2013).

7.2.2. Secondary reference standards

We recommend regular analysis of commercially available secondary water standards (e.g., GISP and USGS reference waters) to ensure proper calibration to the VSMOW-SLAP scale, evaluate the accuracy and precision of isotopic measurements, and monitor analytical drift. The ^{18}O and ^2H values of GISP and USGS reference water are readily available (Araguas-Araguas and Rozanski, 1995; Brand et al., 2014; Gonfiantini, 1984); presently, values of ^{17}O and $\Delta^{17}\text{O}$ are only reported by individual laboratories. Isotopic compositions (^{18}O , ^{17}O , ^2H , and $\Delta^{17}\text{O}$) of international and secondary reference waters are summarized in Table 9. Additional information about the USGS reference waters in Table 9 are available in USGS reports on the isotopic composition of reference materials (Report of Stable Isotopic Composition Reference Material USGS45, 2014; Report of Stable Isotopic Composition Reference Material USGS46, 2014; Report of Stable Isotopic Composition Reference Material USGS47, 2014; Report of Stable Isotopic Composition Reference Material USGS48, 2014; Report of Stable Isotopic Composition Reference Material USGS49, 2015; Report of Stable Isotopic Composition Reference Material USGS50, 2015).

In our experience, ~ 5–10% of samples within an analytical session should be secondary reference waters. This proportion is necessary for a meaningful assessment of the accuracy and precision of data, although more USGS and/or GISP analyses may be necessary when unknown

sample waters span a large (~ 10‰) range in ^{18}O or d-excess. Secondary reference analyses should be distributed evenly throughout every analytical session to monitor instrument drift.

Finally, the isotopic composition of standards and reference waters should bracket the expected isotopic composition of unknowns. This is typically not an issue for ^{18}O , ^{17}O , and ^2H because USGS reference waters span the common range of natural waters (Fig. 4a and c, Table 9). However, the range of $\Delta^{17}\text{O}$ and d-excess of standards and reference waters (Table 9) is much smaller than observed $\Delta^{17}\text{O}$ (Fig. 3b) and d-excess (Fig. 3e) variability. Therefore, we recommend that laboratories develop additional internal reference waters to expand isotopic ranges. New reference waters can be developed from evaporated snow or creative collections of combustion water (e.g., condensate from a home furnace) that have very low (~ 350 per meg) $\Delta^{17}\text{O}$ values that inherit oxygen from atmospheric O_2 ($\Delta^{17}\text{O} \sim 400$ to 500 per meg) (Barkan and Luz, 2011; Wostbrock et al., 2020; Yeung et al., 2012; Young et al., 2014).

7.2.3. Analytical sanity checks

We recommend laboratories perform evaporation experiments and develop mixing curves to monitor analytical performance. Laboratory-controlled evaporation and mixing experiments can result in substantial isotopic variation (far above analytical precision) and are well-predicted by common isotope models (for example, Eqs. (10) and (11)). These quality checks are relatively simple and should be included as part of regular analytical maintenance and upkeep. Code to calculate isotopic variation during mixing and evaporation experiments is provided in Supplements 5 and 6, respectively.

7.2.4. Analytical $\Delta^{17}\text{O}$ precision

Typical reported precision for $\Delta^{17}\text{O}$ (~ 10 per meg) is orders of magnitude better than analytical errors in ^{17}O and ^{18}O (~ 0.1 to 1‰). One major source of analytical error in both IRMS and laser absorption spectrometers is physical fractionation of water vapor during sample handling (i.e., injection, sample conversion, and transport of the vapor to optical cavities or through O_2 prep lines). However, this fractionation is presumably mass-dependent and ^{18}O and ^{17}O errors are very highly correlated along a line with a slope close to 0.528, resulting in very

precise $\Delta^{17}\text{O}$ measurements (Barkan and Luz, 2007; Landais et al., 2006; Schauer et al., 2016; Schoenemann et al., 2013; Steig et al., 2014). In other words, if ^{18}O and ^{17}O vary during sample handling, they do so along a line that is parallel to ϵ_{ref} (0.528) and $\Delta^{17}\text{O}$ errors are largely independent of the precision for ^{18}O and ^{17}O .

Achieving sufficiently high (~ 10 per meg or better) $\Delta^{17}\text{O}$ precision can be an analytical challenge, but is necessary in hydrologic triple oxygen isotope studies because the natural $\Delta^{17}\text{O}$ variability of most meteoric waters (Fig. 3b) is not much greater than analytical $\Delta^{17}\text{O}$ precision. On IRMS systems, sufficient $\Delta^{17}\text{O}$ precision is achieved by careful sample preparation and well-tuned isotopic analysis as described in Section 8.2. With laser absorption spectrometers, high $\Delta^{17}\text{O}$ precision can be achieved with a long (up to 20 minutes) integration time on each injection (Schauer et al., 2016; Steig et al., 2014) or many (> 20) repeat analyses of the same sample (e.g., Berman et al., 2013).

Currently, there is no universal way to calculate and report the analytical precision and accuracy of triple oxygen isotope measurements. For example, some studies use the pooled standard deviation of secondary reference waters to report analytical precision (e.g., Landais et al., 2010; Li et al., 2015) while others use the root mean square error of replicate analyses to report analytical precision and accuracy (e.g., Schauer et al., 2016; Bershaw et al., 2020). The pooled standard deviation (σ_p) is:

$$\sqrt{\frac{\sum s_i^2}{k}} \quad (17)$$

where s_i is the standard deviation and n_i is the number of replicate measurements of the i -th sample and k is the total number of samples. The root mean square error (RMSE) is:

$$\sqrt{\frac{\sum (y_i - \hat{y}_i)^2}{k}} \quad (18)$$

where y_i is the observed isotopic composition, \hat{y}_i is the accepted isotopic composition, and k is the total number of samples. Preferences among these (and other) statistical reporting techniques vary among laboratories and researchers, so we highlight the most important principles in $\Delta^{17}\text{O}$ error reporting and leave the particular approach or statistical test to the discretion of individual authors.

At a minimum, triple oxygen isotope papers should report analytical precision and accuracy, explain any drift and/or memory corrections that were used to correct ^{18}O or ^{17}O data, state which standards were used to normalize the data and the number of replicate analyses of both standards and unknowns, and clearly articulate the value of ϵ_{ref} used to calculate $\Delta^{17}\text{O}$. For example, we report this analytical information in Section 8.2 alongside our analytical methods, state the value of ϵ_{ref} in Section 4.1 as part of our description of the new surface water dataset, and include the number of replicate analyses in the Supplements 1–3.

Finally, we note the important distinction between analytical error (reported as the pooled standard deviation, root mean square error, etc.) and the uncertainty of individual samples (typically reported as one standard deviation for replicate analyses of unknowns). It is important to differentiate these measures of uncertainty because the analytical error represents the performance of the analytical system while the standard deviation of analyses represents error on each unknown.

7.2.5. Isotopic reporting recommendations

First and foremost, it is imperative that triple oxygen isotope data are reported to three decimal places to calculate $\Delta^{17}\text{O}$ and facilitate data comparisons. For every sample, data can be reported as ^{18}O and ^{17}O from individual analyses, both to three decimal places, or as average ^{18}O and average $\Delta^{17}\text{O}$ from multiple analyses, both to three decimal places (Schoenemann et al., 2013). Supplements 1–3 are included as templates to report unknown, standard, and reference water data.

Following precedent set by early triple oxygen isotope studies

(Barkan and Luz, 2007; Luz and Barkan, 2010), we recommend that $\Delta^{17}\text{O}$ be calculated with a value of 0.528 for ϵ_{ref} . This value maintains consistency with previous work (Table 2), clearly distinguishes equilibrium ($\epsilon_{\text{eq}} = 0.529$) and kinetic ($\epsilon_{\text{diff}} = 0.518$) fractionation effects (Fig. 14), and removes most $\Delta^{17}\text{O}$ effects from Rayleigh distillation.

Finally, we recommend that triple oxygen water isotope studies include both $\Delta^{17}\text{O}$ and d-excess data when possible. Combining $\Delta^{17}\text{O}$ and d-excess can reveal information about hydrologic cycling (Section 6) and the parameters (e.g., ϵ_{ref} , ϵ_{eq} , and ϵ_{diff} values) that drive isotope fractionation. Adding ^2H measurements is straightforward for studies that use laser absorption spectrometers and is a worthwhile additional measurement for those that use IRMS techniques.

7.2.6. Memory effects

Regardless of analytical method (IRMS or laser absorption spectroscopy), we recommend analyzing samples in order of increasing or decreasing ^{18}O and using preparatory injections to minimize memory effects. As needed, USGS reference waters can help bridge large ^{18}O gaps between sequential samples. In Picarro and LGR analyzers, the isotopic compositions of water from preparatory injections are analyzed but the data are typically ignored (e.g., Bailey et al., 2013; Berman et al., 2013; Schauer et al., 2016; Steig et al., 2014; Tian et al., 2018). In IRMS systems, memory effects are concentrated in the CoF_3 reactor (Barkan and Luz, 2005) and can be cleared with preparatory injections. Product gases (O_2 and HF) from these injections should be pumped away without purification or analysis.

In our reactors at the University of Michigan, we use one preparatory injection when sequential ^{18}O values are within 5‰, and two preparatory injections when sequential ^{18}O values differ by more than 5‰. In our experience, typically no more than two preparatory injections are necessary to clear IRMS memory effects, but we encourage each lab to independently determine best practices to minimize memory effects from individual reactors.

7.2.7. Sample selection

We recommend using existing ^{18}O and d-excess data to select samples for triple oxygen isotope analysis. For example, at the University of Michigan, we use a Picarro water isotope analyzer to relatively quickly measure ^{18}O and ^2H values, and then systematically select a subset of samples for the much more laborious and time intensive IRMS ^{18}O and ^{17}O analyses. Initial ^{18}O data should also be used to determine the requisite number of preparatory injections and to arrange analytical order to minimize memory effects on $\Delta^{17}\text{O}$.

Sample selection should also consider the expected range of $\Delta^{17}\text{O}$ variation and be sure to select samples that are likely to result in statistically significant $\Delta^{17}\text{O}$ variation (i.e., greater than ~ 10 per meg). For example, assuming non-steady-state evaporation, the maximum possible slope between d-excess and $\Delta^{17}\text{O}$ is ~ 2 per meg ‰ $^{-1}$ (e.g., Barkan and Luz, 2007; Li et al., 2015). Therefore, statistically significant $\Delta^{17}\text{O}$ variation is most probable among samples with more than 5‰ variation in d-excess. Datasets with only a few per mil variability in ^{18}O and/or d-excess typically result in $\Delta^{17}\text{O}$ variation within analytical precision. We encourage researchers to explore the expected $\Delta^{17}\text{O}$ variability on a case-by-case basis with code in Supplement 4.

8. Analytical methods for the new surface water data

As part of this review, we report a new, near-global dataset of surface water triple oxygen isotope data (Figs. 2–4 and 6). A brief summary of our results is in Section 4. Here, we explain our sample collection and analytical methods to give a sense of the IRMS workflow to make accurate and precise $\Delta^{17}\text{O}$ measurements.

8.1. Sample collection

We organized a crowdsourcing effort to collect over 1,600 water

samples from around the world for isotope analysis. Water was collected in 2 dram glass vials (Ace Glass 8779-20) or 20 ml HDPE plastic vials (Wheaton 986716). Samples collected in plastic vials were transferred into glass vials within a few months of collection so we do not expect any fractionation with the sample containers (Spangenberg, 2012). Vials were capped with PolyCone caps to prevent leaks or evaporation, filtered (0.45 μ m, VWR 28145-493), and stored in a dark environment before isotopic analysis.

8.2. Isotopic analysis

We used a Picarro L2130-i cavity ringdown spectrometer with a high-precision vaporizer (A0211) and attached autosampler to measure the ^{18}O and ^2H values of every freshwater sample collected (over 1,500 samples). The L2130-i does not measure ^{17}O . Each sample was analyzed nine times; we use the average of the last four analyses. We used the Picarro ChemCorrect software to monitor samples for organic contamination and normalized measured ^{18}O and ^2H to the VSMOW-SLAP scale with USGS reference waters (USGS45, 46, 49, and 50) and four in-house liquid standards. Isotopic drift and precision were monitored using the Picarro L2130-i Drift and Precision Test worksheet, which is available for download from the Picarro community support forum (<https://www.picarro.com/support/community>). Precision of repeat analyses of deionized water was better than 0.1‰ and 0.3‰ for ^{18}O and ^2H , respectively.

Using the Picarro data, we selected 104 samples (rivers and lakes) from the crowdsourced dataset for triple oxygen isotope analysis. Samples were selected from 17 Koppen climate classes across 6 continents and span 30‰ in ^{18}O and 50‰ in d-excess.

Triple oxygen isotopes were analyzed with a dual inlet Nu Perspective isotope ratio mass spectrometer. We convert liquid water to O_2 gas with cobalt(III) fluoride and a custom-built fluorination line based on the method outlined by Baker et al. (2002) and refined by Luz and Barkan (2010). Our analytical methods have been described previously (Li et al., 2017; Li et al., 2015; Passey et al., 2014), although these measurements were made with a different mass spectrometer (Thermo 253) and fluorination line previously at Johns Hopkins University. Our methods have changed only slightly since the laboratory was relocated to the University of Michigan.

Briefly, we inject ~ 2 L of water through a septum port into a 360–370 C CoF_3 nickel reactor to convert liquid water to O_2 gas and gaseous hydrofluoric acid (HF) (Eq. (16)). Helium gas carries O_2 gas through a nickel trap immersed in liquid nitrogen (-196 C) to remove HF. O_2 gas is further purified by passing through a custom-built stainless steel column (~ 1 m, 1/8" OD) that is packed with a 5 Å molecular sieve (Strem Chemicals, CAS#69912-79-4) and immersed in a methanol/dry ice slush (-80 C). After purification, the O_2 gas collects in a -196 C trap that is packed with a 5 Å molecular sieve. This process takes ~ 15 minutes. After the O_2 is collected, helium gas is pumped away (14 minutes), liquid nitrogen is replaced by a -80 C methanol/dry ice slush, and the O_2 is transferred to a -180 C cold finger (12 minutes) that is part of the dual inlet system of the Nu mass spectrometer. The cold finger has a few pellets of 5 Å molecular sieve to ensure the O_2 gas remains in the cold finger. Finally, the cold finger is heated (9 minutes) to 90 C to release O_2 from the molecular sieve, and the sample is introduced to the mass spectrometer. In total, sample preparation takes just over an hour.

The O_2 gas is analyzed in dual inlet mode for m/z 32, 33, and 34. To minimize analytical error, each analysis consists of 40 cycles during which the ratio of sample to reference gas (99.999% compressed oxygen, with approximate values of $^{17}\text{O}_{\text{VSMOW}} = 10.3\%$, $^{18}\text{O}_{\text{VSMOW}} = 20.3\%$) is determined. Each cycle consists of 50 seconds of integration time on the sample gas or reference gas and 20 seconds of idle time between integrations. Resistances on the m/z 32, 33, and 34 Faraday

cups are 2×10^8 , 3×10^{11} , and $1 \times 10^{11} \Omega$, respectively. Analysis in the mass spectrometer takes approximately two hours.

Triple oxygen isotope data are normalized to the VSMOW-SLAP scale following the approach described by Schoenemann et al. (2013). We analyze VSMOW2 and SLAP2 in at least triplicate at the beginning, end, and middle of every reactor, and routinely analyze six USGS reference waters (USGS45, 46, 47, 48, 49, 50) to determine long-term, external precision of our system, to monitor isotopic drift, and to ensure analytical accuracy. The root mean square error of replicate triple oxygen isotope analyses of USGS reference waters in our lab is 0.3‰ for ^{17}O , 0.9‰ for ^{18}O , and 10 per meg for $\Delta^{17}\text{O}$.

9. Applications and directions of future work

9.1. Modern applications

Studies of $\Delta^{17}\text{O}$ variation in the hydrosphere have two primary applications: as a complement to d-excess and as an analog to the geologic record. In modern hydrologic studies, $\Delta^{17}\text{O}$ and d-excess can provide complementary information about moisture transport and moisture source conditions because $\Delta^{17}\text{O}$ is less sensitive to temperature than d-excess (Fig. 14). For example, a combination of $\Delta^{17}\text{O}$ and d-excess can decouple equilibrium and kinetic fractionation effects and reconstruct both temperature and relative humidity at a moisture source (e.g., Landais et al., 2012a; Uechi and Uemura, 2019).

It is also important to continue to study modern meteoric water $\Delta^{17}\text{O}$ variability in order to improve and expand its use. Geologic and paleoclimate applications of $\Delta^{17}\text{O}$ are very appealing, but it is important to first understand hydrologic $\Delta^{17}\text{O}$ variability, especially of unevaporated waters. Future hydrologic triple oxygen isotope studies should focus on rivers and/or amount-weighted monthly precipitation to evaluate ^{18}O – ^{17}O regression lines and refine our understanding of spatio-temporal $\Delta^{17}\text{O}$ variability. Tap waters were a useful starting point to understand $\Delta^{17}\text{O}$ variation (Li et al., 2015; Tian et al., 2019), but these data can be complicated by non-local isotopic signals so future work should prioritize natural meteoric waters (e.g., precipitation, surface and subsurface water, or snow and ice).

In addition to $\Delta^{17}\text{O}$ studies from long-term precipitation collections, there is a particular need for studies that focus on understanding $\Delta^{17}\text{O}$ variation in convective precipitation. This work is critical to explain $\Delta^{17}\text{O}$ variation of mid- and low-latitude precipitation (e.g., Landais et al., 2010; Li et al., 2015). For example, $\Delta^{17}\text{O}$ values of convective precipitation may decrease due to mixing and/or sub-cloud evaporation or may increase if evaporated vapor re-condenses. Currently, the balance of these effects is not clear in observational (Landais et al., 2010) or modeling (Risi et al., 2010, 2013) studies because there has been relatively little work in this area and the frequency of sample collection (sub-event, event, daily, monthly, etc.) is inconsistent.

Future work is also needed in lake systems to constrain the parameters in isotopic evaporation models (Eqs. (10) and (11)). Observations of water vapor $\Delta^{17}\text{O}$ will be especially important for this because isotopic models of evaporation are very sensitive to the isotopic composition of water vapor (e.g., Gazquez et al., 2018; Gonfiantini et al., 2018; Passey and Ji, 2019), but very little is known about vapor $\Delta^{17}\text{O}$. Lake studies in humid and seasonally dry regions will also be helpful because to date most $\Delta^{17}\text{O}$ lake work has focused on hyperarid climates where lakes are very evaporated (e.g., western US (Passey and Ji, 2019), the Atacama Desert, and Sistan Basin in eastern Iran (Surma et al., 2018, Surma et al., 2015, respectively)). Finally, we encourage data-model comparisons now that many state-of-the-art isotope-enabled general circulation models include ^{17}O (e.g., Brady et al., 2019). This type of work can fill in missing gaps from the observational record and improve our understanding of kinetic fractionation and $\Delta^{17}\text{O}$ variability (Risi

et al., 2013; Schoenemann and Steig, 2016; Wong et al., 2017).

Future modern triple oxygen isotope studies should also expand to include water types that have not yet been studied. These include, but are not limited to, 1) water vapor, which is an important component of isotopic models of evaporation and may affect precipitation $\Delta^{17}\text{O}$ in regions with convective precipitation or a high degree of moisture recycling; 2) soil water, which frequently undergoes extensive fractionation in the upper soil layers (Barnes and Allison, 1984); 3) groundwater, which can integrate information about seasonal recharge, local and regional water tables, and paleoclimate conditions (Jasechko, 2019); and 4) seawater. Generally it is assumed that the isotopic composition of seawater is invariant and similar to that of VSMOW (Luz and Barkan, 2010; Zakharov et al., 2019), but this idea is largely untested for triple oxygen isotopes.

9.2. Paleoclimate and geologic applications

The most appealing application of triple oxygen isotopes in the geologic record is the ability to track aridity and constrain the isotopic effects of evaporation. This has long been a challenge in isotope geochemistry because very few minerals contain both oxygen and hydrogen, and there has not been a d-excess equivalent in geologic materials. Now, the addition of $\Delta^{17}\text{O}$ to geologic ^{18}O records can help identify effects of evaporation and aridity (Alexandre et al., 2019; Gazquez et al., 2018; Passey et al., 2014; Surma et al., 2018), add constraints on diagenesis and formation conditions of sedimentary records (Levin et al., 2014), and reconstruct the isotopic composition of ancient meteoric and ocean waters (e.g., Gehler et al., 2011; Herwartz et al., 2015; Liljestrand et al., 2020; Passey and Ji, 2019). For example, $\Delta^{17}\text{O}$ and 'clumped isotopes' (Δ_{47}) in lake carbonates can be used to reconstruct the isotopic composition of unevaporated paleo-water (Passey and Ji, 2019). Similarly, $\Delta^{17}\text{O}$ from gypsum hydration water offers new insights into changes in relative humidity across glacial-interglacial cycles that are impossible to discern with records of ^{18}O alone (Gazquez et al., 2018).

To date, $\Delta^{17}\text{O}$ has been measured in carbonates, sulfates, phosphates, nitrates, silicates, and oxides to answer an array of paleoclimate questions (Bao et al., 2016). Additional work is still needed to calibrate solid $\Delta^{17}\text{O}$ standards (Barkan et al., 2019; Wostbrock et al., 2020), define fractionation factors (Bergel et al., 2020; Cao and Liu, 2011; Guo and Zhou, 2019; Sharp et al., 2016; Voarintsoa et al., 2020), and refine analytical methods (Affek and Barkan, 2018; Fosu et al., 2020; Sakai et al., 2017), but the potential of triple oxygen isotopes to separate equilibrium and kinetic fractionation effects in paleoclimate applications is immense. Additional work to understand the modern variation in $\Delta^{17}\text{O}$ of both evaporated and unevaporated waters will help expand triple oxygen isotopes as tool for paleoclimate reconstructions.

10. Conclusion

Measurements of small, mass-dependent triple oxygen isotope variations have come a long way in less than two decades. Deviations from a ^{18}O – ^{17}O mass-dependent reference line that were once considered unimportant and too difficult to measure are now well characterized and can separate equilibrium and kinetic fractionation effects. Building upon previous work, this review presents a compilation of new and published meteoric water triple oxygen isotope data. These data do not fit a single ^{18}O – ^{17}O global meteoric water line, which means that triple oxygen isotopes may be sensitive to hydrologic processes that do not dominate equally across the globe. In hydrologic applications, $\Delta^{17}\text{O}$ complements d-excess and adds information about moisture transport, rainout, and evaporation that is impossible to quantify with ^{18}O alone. In paleoclimate applications, $\Delta^{17}\text{O}$ can constrain evaporation and help reconstruct relative humidity or the isotopic composition of paleo-waters. Uncertainties remain about the effects of convective precipitation on $\Delta^{17}\text{O}$ and the spatiotemporal variability of $\Delta^{17}\text{O}$. Additionally, many

water types remain understudied, and future triple oxygen isotope measurements should focus on surface waters and amount-weighted monthly precipitation. This future work will further evaluate meteoric water ^{18}O – ^{17}O relationships and expand the utility of $\Delta^{17}\text{O}$ in hydrologic and paleoclimate applications.

Data availability

All new isotope data associated with this review are included in Supplements 1–3 and are available from the University of Utah Water Isotope Database (<https://wateriso.utah.edu/waterisotopes/>). R scripts (Supplements 4, 5, 6, and 7) and the example raw data file (Supplement 8) that accompanies Supplement 7 can be downloaded from <https://github.com/phoebearon/17O>.

Declaration of Competing Interest

The authors declare that they have no known competing financial interests or personal relationships that could have appeared to influence the work reported in this paper.

Acknowledgements

This study was supported by the University of Michigan Rackham Predoctoral Fellowship and Department of Earth and Environmental Sciences Turner Award (Aron), NSF Tectonics Program Award 1550101 (Poulsen), NSF-EAR Postdoctoral Fellowship Award 1725621 (Beverly), and start-up funds from the University of Michigan Department of Earth and Environmental Sciences (Levin, Passey). We thank Ryan Horwitz for assistance with triple oxygen isotope analyses, Sarah Katz for her keen editorial eye, and the many individuals who participated in our crowdsourced sample collection. We also thank Editor-in-Chief Michael E. Bottcher, Eric Steig, and two anonymous reviewers for providing helpful and constructive reviews that improved this manuscript.

Appendix A. Supplementary data

Supplementary data to this article can be found online at <https://doi.org/10.1016/j.chemgeo.2020.120026>.

References

- Aemisegger, F., Pfahl, S., Sodemann, H., Lehner, I., Seneviratne, S.I., Wernli, H., 2014. Deuterium excess as a proxy for continental moisture recycling and plant transpiration. *Atmos. Chem. Phys.* 14, 4029–4054. <https://doi.org/10.5194/acp-14-4029-2014>.
- Affek, H.P., Barkan, E., 2018. A new method for high-precision measurements of $^{17}\text{O}/^{16}\text{O}$ ratios in H_2O . *Rapid Commun. Mass Spectrom.* 32, 2096–2097. <https://doi.org/10.1002/rcm.8290>.
- Affolter, S., Hauselmann, A.D., Fleitmann, D., Hauselmann, P., Leuenberger, M., 2015. Triple isotope (D, ^{17}O , ^{18}O) study on precipitation, drip water and speleothem fluid inclusions for a Western Central European cave (NW Switzerland). *Quat. Sci. Rev.* 127, 73–89. <https://doi.org/10.1016/j.quascirev.2015.08.030>.
- Alexandre, A., Webb, E., Landais, A., Piel, C., Devidal, S., Sonzogni, C., Couapel, M., Mazur, J.-C., Pierre, M., Prie, F., Vallet-Coulomb, C., Roy, J., 2019. Effects of grass leaf anatomy, development and light/dark alternation on the triple oxygen isotope signature of leaf water and phytoliths: insights for a new proxy of continental atmospheric humidity. *Biogeosciences* 16, 4613–4625. <https://doi.org/10.5194/bg-2019-73>.
- Angert, A., Cappa, C.D., DePaolo, D.J., 2004. Kinetic ^{17}O effects in the hydrologic cycle: indirect evidence and implications. *Geochim. Cosmochim. Acta* 68, 3487–3495. <https://doi.org/10.1016/j.gca.2004.02.010>.
- Araguas-Araguas, L., Rozanski, K., 1995. Interlaboratory comparison for deuterium and oxygen-18 analysis of precipitation samples. Vienna.
- Bailey, A., Toohey, D., Noone, D., 2013. Characterizing moisture exchange between the Hawaiian convective boundary layer and free troposphere using stable isotopes in water. *J. Geophys. Res. Atmos.* 118, 8208–8221. <https://doi.org/10.1002/jgrd.50639>.
- Baker, L., Franchi, I.A., Maynard, J., Wright, I.P., Pillinger, C.T., 2002. A technique for the determination of $^{18}\text{O}/^{16}\text{O}$ and $^{17}\text{O}/^{16}\text{O}$ isotopic ratios in water from small liquid and solid samples. *Anal. Chem.* 74, 1665–1673. <https://doi.org/10.1021/ac010509s>.

- Bao, H., Fairchild, I.J., Wynn, P.M., Spotl, C., 2009. Stretching the Envelope of Past Surface Environments: Neoproterozoic Glacial Lakes from Svalbard. *Science* 323, 119–122.
- Bao, H., Cao, X., Hayles, J.A., 2016. Triple oxygen isotopes: fundamental relationships and applications. *Annu. Rev. Earth Planet. Sci.* 44, 463–492. <https://doi.org/10.1146/annurev-earth-060115-012340>.
- Barkan, E., Luz, B., 2005. High precision measurements of $^{17}\text{O}/^{16}\text{O}$ and $^{18}\text{O}/^{16}\text{O}$ ratios in H_2O . *Rapid Commun. Mass Spectrom.* 19, 3737–3742. <https://doi.org/10.1002/rcm.2250>.
- Barkan, E., Luz, B., 2007. Diffusivity fractionations of $\text{H}_2^{16}\text{O}/\text{H}_2^{17}\text{O}$ and $\text{H}_2^{16}\text{O}/\text{H}_2^{18}\text{O}$ in air and their implications for isotope hydrology. *Rapid Commun. Mass Spectrom.* 21, 2999–3005. <https://doi.org/10.1002/rcm.3180>.
- Barkan, E., Luz, B., 2011. The relationships among the three stable isotopes of oxygen in air, seawater and marine photosynthesis. *Rapid Commun. Mass Spectrom.* 25, 2367–2369. <https://doi.org/10.1002/rcm.5125>.
- Barkan, E., Affek, H., Luz, B., Bergel, S.J., Voarintsoa, N.R.G., Musan, I., 2019. Calibration of ^{17}O and $^{17}\text{O}_{\text{excess}}$ values of three international standards: IAEA-603, NBS19 and NBS18. *Rapid Commun. Mass Spectrom.* 33, 737–740. <https://doi.org/10.1002/rcm.8391>.
- Barnes, C.J., Allison, G., 1984. The distribution of deuterium and ^{18}O in dry soils: 3. Theory for non-isothermal water movement. *J. Hydrol.* 74, 119–135. [https://doi.org/10.1016/0022-1694\(84\)90144-6](https://doi.org/10.1016/0022-1694(84)90144-6).
- Bergel, S.J., Barkan, E., Stein, M., Affek, H.P., 2020. Carbonate $^{17}\text{O}_{\text{excess}}$ as a paleo-hydrology proxy: Triple oxygen isotope fractionation between H_2O and biogenic aragonite, derived from freshwater mollusks. *Geochim. Cosmochim. Acta.* 275, 36–47. <https://doi.org/10.1016/j.gca.2020.02.005>.
- Berman, E.S.F., Levin, N.E., Landais, A., Li, S., Owano, T., 2013. Measurement of ^{18}O , ^{17}O , and ^{17}O -excess in Water by Off-Axis Integrated Cavity Output Spectroscopy and Isotope Ratio Mass Spectrometry. *Anal. Chem.* <https://doi.org/10.1021/ac402366t>.
- Bershaw, J., Hansen, D.D., Schauer, A.J., 2020. Deuterium excess and ^{17}O -excess variability in meteoric water across the Pacific Northwest, USA. *Tellus B Chem. Phys. Meteorol.* 72 (1), 1–17. <https://doi.org/10.1080/16000889.2020.1773722>.
- Bhattacharya, S.K., Savarino, J., Thiemens, M.H., 2000. A new class of oxygen isotopic fractionation in photodissociation of carbon dioxide: Potential implications for atmospheres of Mars and Earth. *Geophys. Res. Lett.* 27, 1459–1462. <https://doi.org/10.1029/1999GL010793>.
- Blunier, T., Barnett, B., Bender, M.L., Hendricks, M.B., 2002. Biological oxygen productivity during the last 60,000 years from triple oxygen isotope measurements. *Global Biogeochem. Cycles* 16, 1–15. <https://doi.org/10.1029/2001gb001460>.
- Blunier, T., Bender, M.L., Barnett, B., Von Fischer, J.C., 2012. Planetary fertility during the past 400 ka based on the triple isotope composition of O_2 in trapped gases from the Vostok ice core. *Clim. Past* 8, 1509–1526. <https://doi.org/10.5194/cp-8-1509-2012>.
- Bowen, G.J., 2010. Isoscapes: spatial pattern in isotopic biogeochemistry. *Annu. Rev. Earth Planet. Sci.* 38, 161–187. <https://doi.org/10.1146/annurev-earth-040809-152429>.
- Bowen, G.J., Cai, Z., Fiorella, R.P., Putman, A.L., 2019. Isotopes in the water cycle: regional- to global-scale patterns and applications. *Annu. Rev.* 47, 453–479. <https://doi.org/10.1146/annurev-earth-053018-060220>.
- Brady, E., Stevenson, S., Bailey, D., Liu, Z., Noone, D., Nusbaumer, J., 2019. The connected isotopic water cycle in the community earth system model version 1. *J. Adv. Model. Earth Syst.* 11, 2547–2566. <https://doi.org/10.1029/2019MS001663>.
- Brand, W.A., Coplen, T.B., 2001. An interlaboratory study to test instrument performance of hydrogen dual-inlet isotope-ratio mass spectrometers. *Fresenius J. Anal. Chem.* 370, 358–362. <https://doi.org/10.1007/s002160100814>.
- Brand, W.A., Coplen, T.B., Vogl, J., Rosner, M., Prohaska, T., 2014. Assessment of international reference materials for isotope-ratio analysis (IUPAC technical report). *Pure Appl. Chem.* 86, 425–467. <https://doi.org/10.1515/pac-2013-1023>.
- Brooks, J.R., Barnard, H.R., Coulombe, R., McDonnell, J.J., 2010. Ecohydrologic separation of water between trees and streams in a Mediterranean climate. *Nat. Geosci.* 3, 100–104. <https://doi.org/10.1038/NGEO722>.
- Cao, X., Liu, Y., 2011. Equilibrium mass-dependent fractionation relationships for triple oxygen isotopes. *Geochim. Cosmochim. Acta* 75, 7435–7445. <https://doi.org/10.1016/j.gca.2011.09.048>.
- Cernusak, L.A., Barbour, M.M., Arndt, S.K., Cheesman, A.W., English, N.B., Feild, T.S., Helliker, B.R., Holloway-Phillips, M.M., Holtum, J.A.M., Kahmen, A., Mcinerney, F.A., Munksgaard, N.C., Simonin, K.A., Song, X., Stuart-Williams, H., West, J.B., Farquhar, G.D., 2016. Stable isotopes in leaf water of terrestrial plants. *Plant Cell Environ.* 39, 1087–1102. <https://doi.org/10.1111/pce.12703>.
- Coplen, T.B., 1988. Normalization of oxygen and hydrogen isotope data. *Chem. Geol. Isot. Geosci. Sect.* 72, 293–297.
- Craig, H., 1961. Isotopic Variations in Meteoric Waters. *Science* 133, 1702–1703. <https://doi.org/10.1126/science.133.3465.1702>.
- Craig, H., Gordon, L.I., 1965. Deuterium and oxygen-18 variations in the ocean and the marine atmosphere. In: Tongiorgi, E. (Ed.), *Proceedings of a Conference on Stable Isotopes in Oceanographic Studies and Paleotemperatures*. Spoleto, Italy, pp. 9–130.
- Criss, R.E., 1999. *Principles of Stable Isotope Distribution*. Oxford University Press, New York.
- Criss, R.E., Farquhar, J., 2008. Abundance, Notation, and Fractionation of Light Stable Isotopes. *Rev. Mineral. Geochemistry* 68, 15–30. <https://doi.org/10.2138/rmg.2008.68.3>.
- Dansgaard, W., 1964. Stable isotopes in precipitation. *Tellus* 16, 436–468. <https://doi.org/10.3402/tellusa.v16i4.8993>.
- Dütsch, M., Pfahl, S., Sodemann, H., 2017. The impact of nonequilibrium and equilibrium fractionation on two different deuterium excess definitions. *J. Geophys. Res. Atmos.* 122, 12732–12746. <https://doi.org/10.1002/2017JD027085>.
- Farquhar, J., Thiemens, M.H., 2000. Oxygen cycle of the Martian atmosphere-regolith system: of secondary phases in Nakhla and Lafayette. *J. Geophys. Res.* 105, 991–997. <https://doi.org/10.1029/1999je001194>.
- Fosu, B.R., Subba, R., Peethambaran, R., Bhattacharya, S.K., Ghosh, P., 2020. Technical note: developments and applications in triple oxygen isotope analysis of carbonates. *ACS Earth Sp. Chem.* 4, 702–710. <https://doi.org/10.1021/acsearthspacechem.9b00330>.
- Franz, P., Rockmann, T., Franz, P., High-precision, T.R., 2005. High-precision isotope measurements of H_2^{16}O , H_2^{17}O , H_2^{18}O , and the $\Delta^{17}\text{O}$ -anomaly of water vapor in the southern lowermost stratosphere. *Atmos. Chem. Phys.* 5, 5373–5403.
- Galewsky, J., Steen-Larsen, H.C., Field, R.D., Worden, J., Risi, C., Schneider, M., 2016. Stable isotopes in atmospheric water vapor and applications to the hydrologic cycle. *Rev. Geophys.* 54, 809–865. <https://doi.org/10.1002/2015RG000512>.
- Gat, J., 1996. Oxygen and hydrogen isotopes in the hydrologic cycle. *Annu. Rev. Earth Planet. Sci.* 24, 225–262. <https://doi.org/10.1146/annurev.earth.24.1.225>.
- Gazquez, F., Calafora, J.M., Evans, N.P., Hodell, D.A., 2017. Using stable isotopes (^{17}O , ^{18}O and D) of gypsum hydration water to ascertain the role of water condensation in the formation of subaerial gypsum speleothems. *Chem. Geol.* 452, 34–46. <https://doi.org/10.1016/j.chemgeo.2017.01.021>.
- Gazquez, F., Morellon, M., Bauska, T., Herwartz, D., Surma, J., Moreno, A., Staubwasser, M., Valero-garces, B., Delgado-huertaa, A., Hodell, D.A., 2018. Triple oxygen and hydrogen isotopes of gypsum hydration water for quantitative paleo-humidity reconstruction. *Earth Planet. Sci. Lett.* 481, 177–188. <https://doi.org/10.1016/j.epsl.2017.10.020>.
- Gehler, A., Tütken, T., Pack, A., 2011. Triple oxygen isotope analysis of bioapatite as tracer for diagenetic alteration of bones and teeth. *Palaeogeogr. Palaeoclimatol. Palaeoecol.* 310, 84–91. <https://doi.org/10.1016/j.palaeo.2011.04.014>.
- Gonfiantini, R., 1978. Standards for stable isotope measurements in natural compounds. *Nature* 271, 534–536. <https://doi.org/10.1038/271534a0>.
- Gonfiantini, R., 1984. Advisory group meeting on stable isotope reference samples for geochemical and hydrochemical investigations. Vienna.
- Gonfiantini, R., Wassenaar, L.L., Araguas-Araguas, L., Aggarwal, P.K., 2018. A unified Craig-Gordon isotope model of stable hydrogen and oxygen isotope fractionation during fresh or saltwater evaporation. *Geochim. Cosmochim. Acta* 235, 224–236. <https://doi.org/10.1016/j.gca.2018.05.020>.
- Guo, W., Zhou, C., 2019. Triple oxygen isotope fractionation in the DIC- H_2O - CO_2 system: A numerical framework and its implications. *Geochim. Cosmochim. Acta* 246, 541–564. <https://doi.org/10.1016/j.gca.2018.11.018>.
- Herwartz, D., Pack, A., Krylov, D., Xiao, Y., Muehlenbachs, K., Sengupta, S., Di Rocco, T., 2015. Revealing the climate of snowball Earth from ^{17}O systematics of hydrothermal rocks. *Proc. Natl. Acad. Sci. U. S. A.* 112, 5337–5341. <https://doi.org/10.1073/pnas.1422887112>.
- Horita, J., Wesolowski, D.J., 1994. Liquid-vapor fractionation of oxygen and hydrogen isotopes of water from the freezing to the critical temperature. *Geochim. Cosmochim. Acta* 58, 3425–3437.
- Hulston, J.R., Thode, H.G., 1965. Variations in the S^{33} , S^{34} , and S^{36} Contents of Meteorites and Their Relation to Chemical and Nuclear Effects. *J. Geophys. Res.* 70, 3475–3484.
- Jasechko, S., 2019. Global Isotope Hydrogeology | Review. *Rev. Geophys.* 57, 835–965. <https://doi.org/10.1029/2018RG000627>.
- Joussame, S., Jouzel, J., Sadourny, R., 1984. A general circulation model of water isotope cycles in the atmosphere. *Nature* 311, 24–29. <https://doi.org/10.1038/311680a0>.
- Jouzel, J., Merlivat, L., 1984. Deuterium and Oxygen 18 in Precipitation: Modeling of the Isotopic Effects During Snow Formation. *J. Geophys. Res.* 89, 11749–11757. <https://doi.org/10.1029/JD089iD07p11749>.
- Kaiser, J., 2009. Reformulated ^{17}O correction of mass spectrometric stable isotope measurements in carbon dioxide and a critical appraisal of historic 'absolute carbon and oxygen isotope ratios. *Geochim. Cosmochim. Acta* 72, 1312–1334. <https://doi.org/10.1016/j.gca.2007.12.011>.
- Kaseke, K.F., Wang, L., Wanke, H., Tian, C., Lanning, M., Jiao, W., 2018. Precipitation Origins and Key Drivers of Precipitation Isotope (^{18}O , ^2H , and ^{17}O) Compositions Over Windhoek. *J. Geophys. Res. Atmos.* 123, 7311–7330. <https://doi.org/10.1029/2018JD028470>.
- Kendall, C., Coplen, T.B., 2001. Distribution of oxygen-18 and deuterium in river waters across the United States. *Hydrol. Process.* 15, 1363–1393. <https://doi.org/10.1002/hyp.217>.
- Landais, A., Barkan, E., Yakir, D., Luz, B., 2006. The triple isotopic composition of oxygen in leaf water. *Geochim. Cosmochim. Acta* 70, 4105–4115. <https://doi.org/10.1016/j.gca.2006.06.1545>.
- Landais, A., Barkan, E., Luz, B., 2008. Record of ^{18}O and ^{17}O -excess in ice from Vostok Antarctica during the last 150,000 years. *Geophys. Res. Lett.* 35, 1–5. <https://doi.org/10.1029/2007GL032096>.
- Landais, A., Risi, C., Bony, S., Vimeux, F., Descroix, L., Falourd, S., Bouyges, A., 2010. Combined measurements of ^{17}O -excess and d-excess in African monsoon precipitation: Implications for evaluating convective parameterizations. *Earth Planet. Sci. Lett.* 298, 104–112. <https://doi.org/10.1016/j.epsl.2010.07.033>.
- Landais, A., Ekaykin, A., Barkan, E., Winkler, R., Luz, B., 2012a. Seasonal variations of ^{17}O -excess and d-excess in snow precipitation at Vostok station, East Antarctica. *J. Glaciol.* 58, 725–733. <https://doi.org/10.3189/2012JoG11J237>.
- Landais, A., Steen-Larsen, H.C., Guillevic, M., Masson-Delmotte, V., Vinther, B., Winkler, R., 2012b. Triple isotopic composition of oxygen in surface snow and water

- vapor at NEEM (Greenland). *Geochim. Cosmochim. Acta* 77, 304–316. <https://doi.org/10.1016/j.gca.2011.11.022>.
- Levin, N.E., Raub, T.D., Dauphas, N., Eiler, J.M., 2014. Triple oxygen isotope variations in sedimentary rocks. *Geochim. Cosmochim. Acta* 139, 173–189. <https://doi.org/10.1016/j.gca.2014.04.034>.
- Li, S., Levin, N.E., Chesson, L.A., 2015. Continental scale variation in ^{17}O -excess of meteoric waters in the United States. *Geochim. Cosmochim. Acta* 164, 110–126. <https://doi.org/10.1016/j.gca.2015.04.047>.
- Li, S., Levin, N.E., Soderberg, K., Dennis, K.J., Caylor, K.K., 2017. Triple oxygen isotope composition of leaf waters in Mpala, central Kenya. *Earth Planet. Sci. Lett.* 468, 38–50. <https://doi.org/10.1016/j.epsl.2017.02.015>.
- Liljestrand, F.L., Knoll, A.H., Tosca, N.J., Cohen, P.A., Macdonald, F.A., Peng, Y., Johnston, D.T., 2020. The triple oxygen isotope composition of Precambrian chert. *Earth Planet. Sci. Lett.* 537, 1–10. <https://doi.org/10.1016/j.epsl.2020.116167>.
- Lin, Y., Clayton, R.N., Groning, M., 2010. Calibration of ^{17}O and ^{18}O of international measurement standards VSMOW, VSMOW2, SLAP, and SLAP2. *Rapid Commun. Mass Spectrom.* 24, 773–776. <https://doi.org/10.1002/rcm.4449>.
- Luz, B., Barkan, E., 2010. Variations of $^{17}\text{O}/^{16}\text{O}$ and $^{18}\text{O}/^{16}\text{O}$ in meteoric waters. *Geochim. Cosmochim. Acta* 74, 6276–6286. <https://doi.org/10.1016/j.gca.2010.08.016>.
- Luz, B., Barkan, E., Yam, R., Shemesh, A., 2009. Fractionation of oxygen and hydrogen isotopes in evaporating water. *Geochim. Cosmochim. Acta* 73, 6697–6703. <https://doi.org/10.1016/j.gca.2009.08.008>.
- Majoube, M., 1971. Oxygen-18 and deuterium fractionation between water and steam. *J. Chem. Phys.* 68, 1432–1436.
- Marrero, T.R., Mason, E.A., 1972. Gaseous diffusion coefficients. *J. Phys. Chem. Ref. Data* 1, 3–118. <https://doi.org/10.1063/1.3253094>.
- Matsuhisa, Y., Goldsmith, J.R., Clayton, R.N., 1978. Mechanisms of hydrothermal crystallization of quartz at 250 °C and 15 kbar. *Geochim. Cosmochim. Acta* 42, 173–182. [https://doi.org/10.1016/0016-7037\(78\)90130-8](https://doi.org/10.1016/0016-7037(78)90130-8).
- McKeegan, K.D., Leshin, L.A., 2001. Stable Isotope Variations in Extraterrestrial Materials. *Rev. Mineral. Geochemistry* 43, 279–318. <https://doi.org/10.2138/gsrmg.43.1.279>.
- McKinney, C.R., McCrea, J.M., Epstein, S., Allen, H.A., Urey, H.C., 1950. Improvements in mass spectrometers for the measurement of small differences in isotope abundance ratios. *Rev. Sci. Instrum.* 21, 724–730. <https://doi.org/10.1063/1.1745698>.
- Meijer, H.A.J., Li, W.J., 1998. The Use of Electrolysis for Accurate ^{17}O and ^{18}O Isotope Measurements in Water. *Isot. Environmental Heal. Stud.* 34, 349–369. <https://doi.org/10.1080/10256019808234072>.
- Meijer, H.A.J., Neubert, R.E.M., Visser, G.H., 2000. Cross contamination in dual inlet isotope ratio mass spectrometers. *Int. J. Mass Spectrom.* 198, 45–61. [https://doi.org/10.1016/S1387-3806\(99\)00266-3](https://doi.org/10.1016/S1387-3806(99)00266-3).
- Merlivat, L., 1978. Molecular diffusivities of H_2^{16}O , HD^{16}O , and H_2^{18}O in gases. *J. Chem. Phys.* 69, 2864–2871. <https://doi.org/10.1063/1.436884>.
- Miller, M.F., 2002. Isotopic fractionation and the quantification of ^{17}O anomalies in the oxygen three-isotope system: an appraisal and geochemical significance. *Geochimica et Cosmochimica Acta* 66 (11), 1889–1991.
- Miller, M.F., 2018. Precipitation regime influence on oxygen triple-isotope distributions in Antarctic precipitation and ice cores. *Earth Planet. Sci. Lett.* 481, 316–327. <https://doi.org/10.1016/j.epsl.2017.10.035>.
- New, M., Lister, D., Hulme, M., Makin, I., 2002. A high-resolution data set of surface climate over global land areas. *Clim. Res.* 21, 1–25.
- Noone, D., Risi, C., Bailey, A., Berkelhammer, M., Brown, D.P., Buening, N., Gregory, S., Nusbaumer, J., Schneider, D., Sykes, J., Vanderwende, B., Wong, J., Meillier, Y., Wolfe, D., 2013. Determining water sources in the boundary layer from tall tower profiles of water vapor and surface water isotope ratios after a snowstorm in Colorado. *Atmos. Chem. Phys.* 13, 1607–1623. <https://doi.org/10.5194/acp-13-1607-2013>.
- Pack, A., Herwartz, D., 2014. The triple oxygen isotope composition of the Earth mantle and understanding $\Delta^{17}\text{O}$ variations in terrestrial rocks and minerals. *Earth Planet. Sci. Lett.* 390, 138–145. <https://doi.org/10.1016/j.epsl.2014.01.017>.
- Pang, H., Hou, S., Landais, A., Masson-Delmotte, V., Prie, F., Steen-Larsen, H.C., Risi, C., Li, Y., Jouzel, J., Wang, Y., He, J., Minster, B., Falourd, S., 2015. Spatial distribution of ^{17}O -excess in surface snow along a traverse from Zhongshan station to Dome A, East Antarctica. *Earth Planet. Sci. Lett.* 414, 126–133. <https://doi.org/10.1016/j.epsl.2015.01.014>.
- Pang, H., Hou, S., Landais, A., Delmotte, V.M., Jouzel, J., 2019. Influence of Summer Sublimation on D , ^{18}O , and ^{17}O in Precipitation, East Antarctica, and Implications for Climate Reconstruction From Ice Cores. *J. Geophys. Res. Atmos.* 124, 7339–7358. <https://doi.org/10.1029/2018JD030218>.
- Passey, B.H., Ji, H., 2019. Triple oxygen isotope signatures of evaporation in lake waters and carbonates: A case study from the western United States. *Earth Planet. Sci. Lett.* 518, 1–12. <https://doi.org/10.1016/j.epsl.2019.04.026>.
- Passey, B.H., Hu, H., Ji, H., Montanari, S., Li, S., Henkes, G.A., Levin, N.E., 2014. Triple oxygen isotopes in biogenic and sedimentary carbonates. *Geochim. Cosmochim. Acta* 141, 1–25. <https://doi.org/10.1016/j.gca.2014.06.006>.
- Paul, D., Skrzypiek, G., Forzls, I., 2007. Normalization of measured stable isotopic compositions to isotope reference scales – a review. *Rapid Commun. Mass Spectrom.* 21, 3006–3014. <https://doi.org/10.1002/rcm.3185>.
- Poulsen, C.J., Ehlers, T.A., Insel, N., 2010. Onset of convective rainfall during gradual late miocene rise of the central andes. *Science* 328, 490–493. <https://doi.org/10.1126/science.1185078>.
- Rech, J.A., Currie, B.S., Jordan, T.E., Riquelme, R., Lehmann, S.B., Kirk-Lawlor, N.E., Li, S., Gooley, J.T., 2019. Massive middle Miocene gypsic paleosols in the Atacama Desert and the formation of the Central Andean rain-shadow. *Earth Planet. Sci. Lett.* 506, 184–194. <https://doi.org/10.1016/j.epsl.2018.10.040>.
- Report of Stable Isotopic Composition Reference Material USGS45. Reston, VA. <https://isotopes.usgs.gov/lab/referencematerials/USGS45.pdf>.
- Report of Stable Isotopic Composition Reference Material USGS46. Reston, VA. <https://isotopes.usgs.gov/lab/referencematerials/USGS46.pdf>.
- Report of Stable Isotopic Composition Reference Material USGS47. Reston, VA. <https://isotopes.usgs.gov/lab/referencematerials/USGS47.pdf>.
- Report of Stable Isotopic Composition Reference Material USGS48. Reston, VA. <https://isotopes.usgs.gov/lab/referencematerials/USGS48.pdf>.
- Report of Stable Isotopic Composition Reference Material USGS49. Reston, VA. <https://isotopes.usgs.gov/lab/referencematerials/USGS49.pdf>.
- Report of Stable Isotopic Composition Reference Material USGS50. Reston, VA. <https://isotopes.usgs.gov/lab/referencematerials/USGS50.pdf>.
- Risi, C., Landais, A., Bony, S., Jouzel, J., Masson-Delmotte, V., Vimeux, F., 2010. Understanding the ^{17}O excess glacial-interglacial variations in Vostok precipitation. *J. Geophys. Res. Atmos.* 115, 1–15. <https://doi.org/10.1029/2008JD011535>.
- Risi, C., Landais, A., Winkler, R., Vimeux, F., 2013. Can we determine what controls the spatio-temporal distribution of d-excess and ^{17}O -excess in precipitation using the LMDZ general circulation model? *Clim. Past* 9, 2173–2193. <https://doi.org/10.5194/cp-9-2173-2013>.
- Roscoe, H.K., Fowler, C.L., Shanklin, J.D., Hill, J.G.T., 2004. Possible long-term changes in stratospheric circulation: Evidence from total ozone measurements at the edge of the Antarctic vortex in early winter. *Q. J. R. Meteorol. Soc.* 130, 1123–1135. <https://doi.org/10.1256/qj.03.70>.
- Rowley, D.B., Garzzone, C.N., 2007. Stable isotope-based paleoaltimetry. *Annu. Rev. Earth Planet. Sci.* 35, 463–508. <https://doi.org/10.1146/annurev.earth.35.031306.140155>.
- Rozanski, K., Araguas-Araguas, L., Gonfiantini, R., 1993. Isotopic Patterns in Modern Global Precipitation. In: Swart, P.K., Lohmann, K.C., Mckenzie, J., Savin, S. (Eds.), *Climate Change in Continental Isotopic Records* Geophysical Monograph Series, 78. American Geophysical Union, Washington, DC, pp. 1–36. <https://doi.org/10.1029/GM078p0001>.
- Rumble, D., Miller, M.F., Franchi, I.A., Greenwood, R.C., 2007. Oxygen three-isotope fractionation lines in terrestrial silicate minerals: An inter-laboratory comparison of hydrothermal quartz and eclogitic garnet. *Geochim. Cosmochim. Acta* 71, 3592–3600. <https://doi.org/10.1016/j.gca.2007.05.011>.
- Sakai, S., Matsuda, S., Hikida, T., Shimono, A., Mcmanus, J.B., Zahniser, M., Nelson, D., Dettman, D.L., Yang, D., Ohkouchi, N., 2017. High-Precision Simultaneous $^{18}\text{O}/^{16}\text{O}$, $^{13}\text{C}/^{12}\text{C}$, and $^{17}\text{O}/^{16}\text{O}$ Analyses for Microgram Quantities of CaCO_3 by Tunable Infrared Laser Absorption Spectroscopy. *Anal. Chem.* 89, 11846–11852. <https://doi.org/10.1021/acs.analchem.7b03582>.
- Salati, E., Dall'Olio, A., Matsui, E., Gat, J.R., 1979. Recycling of water in the Amazon Basin: An isotopic study. *Water Resour. Res.* 15, 1250–1258. <https://doi.org/10.1029/WR015i005p01250>.
- Schauer, A.J., Schoenemann, S.W., Steig, E.J., 2016. Routine high-precision analysis of triple water-isotope ratios using cavity ring-down spectroscopy. *Rapid Commun. Mass Spectrom.* 30, 2059–2069. <https://doi.org/10.1002/rcm.7682>.
- Schoenemann, S.W., Steig, E.J., 2016. Seasonal and spatial variations of ^{17}O -excess and d-excess in Antarctic precipitation: Insights from an intermediate complexity isotope model. *J. Geophys. Res. Atmos.* 121, 11215–11247. <https://doi.org/10.1002/2016JD025117>. Received.
- Schoenemann, S.W., Schauer, A.J., Steig, E.J., 2013. Measurement of SLAP2 and GISP ^{17}O and proposed VSMOW-SLAP normalization for ^{17}O and ^{17}O -excess. *Rapid Commun. Mass Spectrom.* 27, 582–590. <https://doi.org/10.1002/rcm.6486>.
- Schoenemann, S.W., Steig, E.J., Ding, Q., Markle, B.R., Schauer, A.J., 2014. Triple water-isotope record from WAIS Divide, Antarctica: Controls on glacial-interglacial changes in ^{17}O -excess of precipitation. *J. Geophys. Res. Atmos.* 119, 8741–8763. <https://doi.org/10.1002/2014JD021770>. Received.
- Sharp, Z.D., Gibbons, J.A., Maltsev, O., Atudorei, V., Pack, A., Sengupta, S., Shock, E.L., Knauth, L.P., 2016. A calibration of the triple oxygen isotope fractionation in the $\text{SiO}_2\text{-H}_2\text{O}$ system and applications to natural samples. *Geochim. Cosmochim. Acta* 186, 105–119. <https://doi.org/10.1016/j.gca.2016.04.047>.
- Sharp, Z.D., Wostbrock, J.A.G., Pack, A., 2018. Mass-dependent triple oxygen isotope variations in terrestrial materials. *Geochem. Perspect. Lett.* 7, 27–31. <https://doi.org/10.7185/geochemlet.1815>.
- Spangenberg, J.E., 2012. Caution on the storage of waters and aqueous solutions in plastic containers for hydrogen and oxygen stable isotope analysis. *Rapid Commun. Mass Spectrom.* 26, 2627–2636. <https://doi.org/10.1002/rcm.6386>.
- Steig, E.J., Gkinis, V., Schauer, A.J., Schoenemann, S.W., Samek, K., Hoffnagle, J., Dennis, K.J., Tan, S.M., 2014. Calibrated high-precision ^{17}O -excess measurements using cavity ring-down spectroscopy with laser-current-tuned cavity resonance. *Atmos. Meas. Tech.* 7, 2421–2435. <https://doi.org/10.5194/amt-7-2421-2014>.
- Surma, J., Assonov, S., Bolourchi, M.J., Staubwasser, M., 2015. Triple oxygen isotope signatures in evaporated water bodies from the Sistan Oasis, Iran. *Geophys. Res. Lett.* 42, 8456–8462. <https://doi.org/10.1002/2015GL066475>.
- Surma, J., Assonov, S., Herwartz, D., Voigt, C., Staubwasser, M., 2018. The evolution of ^{17}O -excess in surface water of the arid environment during recharge and evaporation. *Sci. Rep.* 8, 1–10. <https://doi.org/10.1038/s41598-018-23151-6>.
- Thiemens, M.H., 2006. History and applications of mass-independent isotope effects. *Annu. Rev. Earth Planet. Sci.* 34, 217–262. <https://doi.org/10.1146/annurev.earth.34.031405.125026>.
- Thiemens, M.H., Heidenreich, J.E., 1983. The mass-independent fractionation of oxygen: A novel isotope effect and its possible cosmochemical implications. *Science* 219, 1073–1075. <https://doi.org/10.1126/science.219.4588.1073>.
- Thiemens, M.H., Jackson, T.L., Brenninkmeijer, C.A.M., 1995. Observation of a mass independent oxygen isotopic composition in terrestrial stratospheric CO_2 , the link to

- ozone chemistry, and the possible occurrence in the Martian atmosphere. *Geophys. Res. Lett.* 22, 255–257. <https://doi.org/10.1029/94GL02996>.
- Thiemens, M.H., Chakraborty, S., Dominguez, G., 2012. The physical chemistry of mass-independent isotope effects and their observation in nature. *Annu. Rev. Phys. Chem.* 63, 155–177. <https://doi.org/10.1146/annurev-physchem-032511-143657>.
- Thompson, M., 2012. Precision in chemical analysis: A critical survey of uses and abuses. *Anal. Methods* 4, 1598–1611. <https://doi.org/10.1039/c2ay25083g>.
- Tian, C., Wang, L., 2019. Data Descriptor: Stable isotope variations of daily precipitation from 2014–2018 in the central United States. *Nature Publishing Group*, 6, 1–8. <https://doi.org/10.1038/sdata.2019.18>.
- Tian, C., Wang, L., Kaseke, K.F., Bird, B.W., 2018. Stable isotope compositions (^2H , ^{18}O and ^{17}O) of rainfall and snowfall in the central United States. *Sci. Rep.* 8, 1–15. <https://doi.org/10.1038/s41598-018-25102-7>.
- Tian, C., Wang, L., Tian, F., Zhao, S., Jiao, W., 2019. Spatial and temporal variations of tap water ^{17}O -excess in China. *Geochim. Cosmochim. Acta* 260, 1–14. <https://doi.org/10.1016/j.gca.2019.06.015>.
- Touzeau, A., Landais, A., Stenni, B., Uemura, R., Fukui, K., Fujita, S., Guilbaud, S., Ekaykin, A., Casado, M., Barkan, E., Luz, B., Magand, O., Teste, G., Le Meur, E., Baroni, M., Savarino, J., Bourgeois, I., Risi, C., 2016. Acquisition of isotopic composition for surface snow in East Antarctica and the links to climatic parameters. *The Cryosphere* 10 (2), 837–852. <https://doi.org/10.5194/tc-10-837-2016>.
- Uechi, Y., Uemura, R., 2019. Dominant influence of the humidity in the moisture source region on the ^{17}O -excess in precipitation on a subtropical island. *Earth Planet. Sci. Lett.* 513, 20–28. <https://doi.org/10.1016/j.epsl.2019.02.012>.
- Uemura, R., Barkan, E., Abe, O., Luz, B., 2010. Triple isotope composition of oxygen in atmospheric water vapor. *Geophys. Res. Lett.* 37, 1–4. <https://doi.org/10.1029/2009GL041960>.
- Uemura, R., Masson-Delmotte, V., Jouzel, J., Landais, A., Motoyama, H., Stenni, B., 2012. Ranges of moisture-source temperature estimated from Antarctic ice cores stable isotope records over glacial-interglacial cycles. *Clim. Past* 8, 1109–1125. <https://doi.org/10.5194/cp-8-1109-2012>.
- Voarintsoa, N.R.G., Barkan, E., Bergel, S., Vieten, R., Affek, H.P., 2020. Triple oxygen isotope fractionation between CaCO_3 and H_2O in inorganically precipitated calcite and aragonite. *Chem. Geol.* 539, 119500. <https://doi.org/10.1016/j.chemgeo.2020.119500>.
- Werner, R.A., Brand, W.A., 2001. Referencing strategies and techniques in stable isotope ratio analysis. *Rapid Commun. Mass Spectrom.* 15, 501–519. <https://doi.org/10.1002/rcm.258>.
- Winkler, R., Landais, A., Sodemann, H., Dümbgen, L., Prie, F., Masson-Delmotte, V., Stenni, B., Jouzel, J., 2012. Deglaciation records of ^{17}O -excess in East Antarctica: Reliable reconstruction of oceanic normalized relative humidity from coastal sites. *Clim. Past* 8, 1–16. <https://doi.org/10.5194/cp-8-1-2012>.
- Wong, T.E., Nusbaumer, J., Noone, D.C., 2017. Evaluation of modeled land-atmosphere exchanges with a comprehensive water isotope fractionation scheme in version 4 of the Community Land Model. *J. Adv. Model. Earth Syst.* 9, 978–1001. <https://doi.org/10.1002/2016MS000842>.
- Wostbrock, J.A.G., Cano, E.J., Sharp, Z.D., 2020. An internally consistent triple oxygen isotope calibration of standards for silicates, carbonates and air relative to VSMOW2 and SLAP2. *Chem. Geol.* 533, 119432. <https://doi.org/10.1016/j.chemgeo.2019.119432>.
- Yeung, L.Y., Young, E.D., Schauble, E.A., 2012. Measurements of $^{18}\text{O}^{18}\text{O}$ and $^{17}\text{O}^{18}\text{O}$ in the atmosphere and the role of isotope-exchange reactions. *J. Geophys. Res. Atmos.* 117, 1–20. <https://doi.org/10.1029/2012JD017992>.
- Yeung, L.Y., Hayles, J.A., Hu, H., Ash, J.L., Sun, T., 2018. Scale distortion from pressure baselines as a source of inaccuracy in triple-isotope measurements. *Rapid Commun. Mass Spectrom.* 32, 1811–1821. <https://doi.org/10.1002/rcm.8247>.
- Young, E.D., Galy, A., 2004. The isotope geochemistry and cosmochemistry of magnesium. *Revs. Mineral. Geochem.* 55, 197–230. <https://doi.org/10.2138/gsrmg.55.1.197>.
- Young, E.D., Galy, A., Nagahara, H., 2002. Kinetic and equilibrium mass-dependent isotope fractionation laws in nature and their geochemical and cosmochemical significance. *Geochim. Cosmochim. Acta* 66, 1095–1104. [https://doi.org/10.1016/S0016-7037\(01\)00832-8](https://doi.org/10.1016/S0016-7037(01)00832-8).
- Young, E.D., Yeung, L.Y., Kohl, I.E., 2014. On the ^{17}O budget of atmospheric O_2 . *Geochim. Cosmochim. Acta* 135, 102–125. <https://doi.org/10.1016/j.gca.2014.03.026>.
- Zachos, J., 2001. Trends, Rhythms, and Aberrations in Global Climate 65 Ma to Present, 292, pp. 686–693. <https://doi.org/10.1126/science.1059412>.
- Zakharov, D.O., Bindeman, I.N., Tanaka, R., Friðleifsson, G.O., Reed, M.H., Hampton, R. L., 2019. Triple oxygen isotope systematics as a tracer of fluids in the crust: A study from modern geothermal systems of Iceland. *Chem. Geol.* 530, 119312. <https://doi.org/10.1016/j.chemgeo.2019.119312>.